Quaternary Science Reviews 339 (2024) 108841

Contents lists available at ScienceDirect

Quaternary Science Reviews

journal homepage: www.elsevier.com/locate/quascirev

Abrupt climate change at the MIS 5/4 transition recorded in a speleothem from the Eastern Mediterranean

Alice R. Paine [a,b,*], James U.L. Baldini [a], Ezgi Ünal-İmer [c], Fabian B. Wadsworth [a], Alexander A. Iveson [a,d], Madeleine C.S. Humphreys [a], Richard J. Brown [a], Wolfgang Müller [e], Christopher J. Ottley [a]

[a] Department of Earth Sciences, Durham University, DH1 3LE, UK
[b] Department of Earth Sciences, University of Oxford, OX1 3AN, UK
[c] Department of Geological Engineering, Middle East Technical University, Ankara, Türkiye
[d] Pacific Northwest National Laboratory, Washington, WA 99352, USA
[e] Institut für Geowissenschaften, Goethe Universität, 60438 Frankfurt am Main, Germany

ARTICLE INFO

Handling Editor: Dominik Fleitmann

Keywords:
Southern Türkiye
Geochemistry
Stadial
Interstadial
Hydroclimate
Caves
Carbonate

ABSTRACT

The marine isotope stage (MIS) 5a to 4 transition (~74 ka) was associated with rapid ice sheet expansion, declining moisture availability globally, and significant upheaval of terrestrial ecosystems across the northern hemisphere. Here, we present precisely dated speleothem trace element records spanning ~90 to 70 ka from Dim Cave (Southern Türkiye) which provide crucial information regarding the climate response to this transition from the Eastern Mediterranean region. Trace element variability recorded in stalagmite DIM-E3 captures shifts in detrital influx, bedrock dissolution, and soil activity that collectively record two climatic signals: (1) high regional moisture availability between MIS 5c and 5b, and (2) increasingly arid conditions across the MIS 5a to MIS 4 transition. Both are contemporaneous with evidence for severe drying recorded across the Eastern Mediterranean and Middle East, as well as Asia, Europe, South America, and the North Atlantic. These results shed new light on the environmental consequences of rapid change in a climatologically sensitive region, and underscore the significance of atmospheric teleconnections in propagation of abrupt climate variability during the last glacial period.

1. Introduction

Understanding the timing, expression, and impacts of climate variability under pre-industrial conditions is a key goal of modern paleoclimatology. Significant attention has been paid to exploring the effects of this variability on global precipitation patterns (Marvel et al., 2019). This is not only because information on past events can directly inform models on which future global climate projections are based, but also due to the severe socioeconomic upheaval that both drought and flood events can cause (Mondal et al., 2023). Model projections forecast large increases in the frequency and intensity of extreme precipitation events across nearly all latitudes as a consequence of rapid, anthropogenically-driven climate warming (Dai, 2013; Martinez-Villalobos and Neelin, 2023). Thus, understanding what triggers these events, the land–atmosphere interactions that drive their severity, and the spatial scales upon which they occur is critically important (Bradley and Diaz, 2021; Mondal et al., 2023).

Naturally occurring archives yield unique insights into the timing, nature, and expression of climate variability many thousands of years into the past. Composite marine (e.g., Lisiecki and Raymo, 2005), ice core (e.g., Brook and Buizert, 2018; Jouzel et al., 2007), and speleothem (e.g., Cheng et al., 2016; Moseley et al., 2014) isotope records suggest the occurrence of five global-scale shifts between cold and warm climate conditions during the last glacial period (~115–11 ka), termed Marine Isotope Stages (MIS) based on their expression in marine sediment stacks. Of the five shifts, the transition from MIS 5 to MIS 4 is particularly intriguing due to its distinct and abrupt 'switch' to severe cold and/or dry conditions affecting the South American Monsoon (Cheng et al., 2013; Cruz et al., 2005; Deplazes et al., 2013), the Indian Monsoon (Fleitmann et al., 2003; Kathayat et al., 2016; Kaushal et al., 2018), the North Atlantic (Camuera et al., 2022; Lisiecki and Raymo, 2005; Rasmussen et al., 2014), and other domains. These conditions were a stark

* Corresponding author. Department of Earth Science, University of Oxford, OX1 3AN, UK.
E-mail address: alice.paine@earth.ox.ac.uk (A.R. Paine).

https://doi.org/10.1016/j.quascirev.2024.108841
Received 25 April 2024; Received in revised form 7 July 2024; Accepted 14 July 2024
Available online 20 July 2024

contrast to warm global temperatures high sea levels during MIS 5e (~130–114 ka) (Past Interglacials Working Group of PAGES, 2016; Regattieri et al., 2016; Stoll et al., 2022). The stable interglacial climate of MIS 5e was followed by heightened variability in temperature, sea level, and environmental conditions during MIS 5d to 5a, prior to the arrival of strong glacial conditions during MIS 4 (Railsback et al., 2015).

The stepwise nature of the MIS 5-to-4 transition calls for a better understanding of its impacts on the function, and structure, of different terrestrial environments; particularly those with heightened sensitivity to global-scale hydroclimate shifts (Mondal et al., 2023). One such region is the Eastern Mediterranean (Fig. 1). Located at the convergence between the northern hemisphere westerlies and the sub-tropical anticyclonic belt, it is a modern-day climate change 'hotspot' experiencing precipitation shifts at a rate almost two times faster than the global average over the past four decades (Kim et al., 2019; Zittis et al., 2022). On pre-industrial timescales, drying in the Eastern Mediterranean broadly corresponds to cooling in the North Atlantic, weakening of the Asian monsoon, and drying in North Africa and mainland Europe (Fleitmann et al., 2009; Mehterian et al., 2017; Rowe et al., 2012; Stockhecke et al., 2016) – suggesting strong teleconnections that could have produced equally severe perturbations in the region across the MIS 5a-to-4 transition (Stockhecke et al., 2016).

Studying the environmental consequences of abrupt climate change in the Eastern Mediterranean is important not only for paleoclimatology, but also for palaeoanthropology. New studies have highlighted the importance of climate as driver of early *Homo sapiens* dispersal out of East Africa and into Eurasia during MIS 5 (Bergström et al., 2021; Beyer et al., 2021; Foerster et al., 2022; Schaebitz et al., 2021; Timmermann et al., 2022), with evidence for hominin and faunal expansions into the Levant corresponding to a wetter climate (Abbas et al., 2023; Bae et al., 2017; Barzilai et al., 2022; Groucutt et al., 2021). A sudden shift to cold and dry glacial conditions could have profoundly influenced the living conditions of these populations, encouraging long-distance migration in search of sufficient food and water (Schaebitz et al., 2021), and instigating distinct anatomical, biological, and cultural adaptations (Foerster et al., 2022). Constraining the timing and expression of this transition in the East Mediterranean could thus provide new perspectives on the conditions under which these early humans lived, as well as a broader understanding of societal responses to abrupt climate variability.

Few paleoclimate records corresponding to MIS 5/4 transition are currently available from the Eastern Mediterranean (Fig. 1). These take the form of low/moderate-resolution sedimentary sequences from the Mediterranean Sea (Ehrmann and Schmiedl, 2021; Grant et al., 2016), terrestrial lakes (Gasse et al., 2015; Litt et al., 2014; Miebach et al., 2019; Stockhecke et al., 2016), or the stable isotope (e.g., $\delta^{18}O$ and/or $\delta^{13}C$) records gleaned from speleothems growing in Karaca (Rowe et al., 2012), Qal'e Kord (Mehterian et al., 2017), Soreq (Bar-Matthews et al., 2003), and Sofular (Held et al., 2024) caves. The latter have demonstrated that the pacing of the speleothem $\delta^{18}O$ shifts are broadly comparable to ice core records, yet also highlight how the climatic signals recorded by isotopes are far from simple to interpret; particularly in this part of the world (e.g., Bar-Matthews et al., 2019; Vaks et al., 2006). For example, low $\delta^{18}O$ values in stalagmites from the west of the Eastern Mediterranean have been interpreted to record surface cooling (Fleitmann et al., 2009; Moseley et al., 2014), changes in moisture source in the north-east (Rowe et al., 2012), the fractional loss of moisture along the continental westerlies storm belt trajectory inland to the east (Carolin et al., 2019; Mehterian et al., 2017), and changes in precipitation amount on the Mediterranean coast (Drysdale et al., 2007). Quantifying trace element variability within these records can directly complement the interpretations gleaned from stable isotopes (Fairchild and Treble, 2009; Kern et al., 2019). Whereas the speleothem's oxygen isotope signal is generally a reflection of atmospheric processes (e.g., precipitation (Wong and Breecker, 2015)), and carbon isotopes of variation in biogenic activity above the cave, water availability, or vegetation type (Lechleitner et al., 2019), speleothem trace element signals are derived from sources that are mainly terrestrial in origin, meaning they can record climate-driven changes in soil conditions, water-bedrock interactions, atmospheric composition inside the cave (e.g., the partial pressure of CO_2), and other environmental conditions (Fairchild and Treble, 2009). This is particularly valuable for climatologically sensitive regions such as the Eastern Mediterranean, where terrestrial conditions are directly influenced by diverse atmospheric circulation patterns and meteorological processes (Zittis et al., 2022).

Here, we present a continuous, decadal-scale resolution record of trace element variability in sample DIM-E3-A: a sub-section of stalagmite DIM-E3 extracted from Dim Cave (36°32′N, 32°06′E), and corresponding to the ~90 and 70 ka interval (Fig. 2). Previous stable isotope

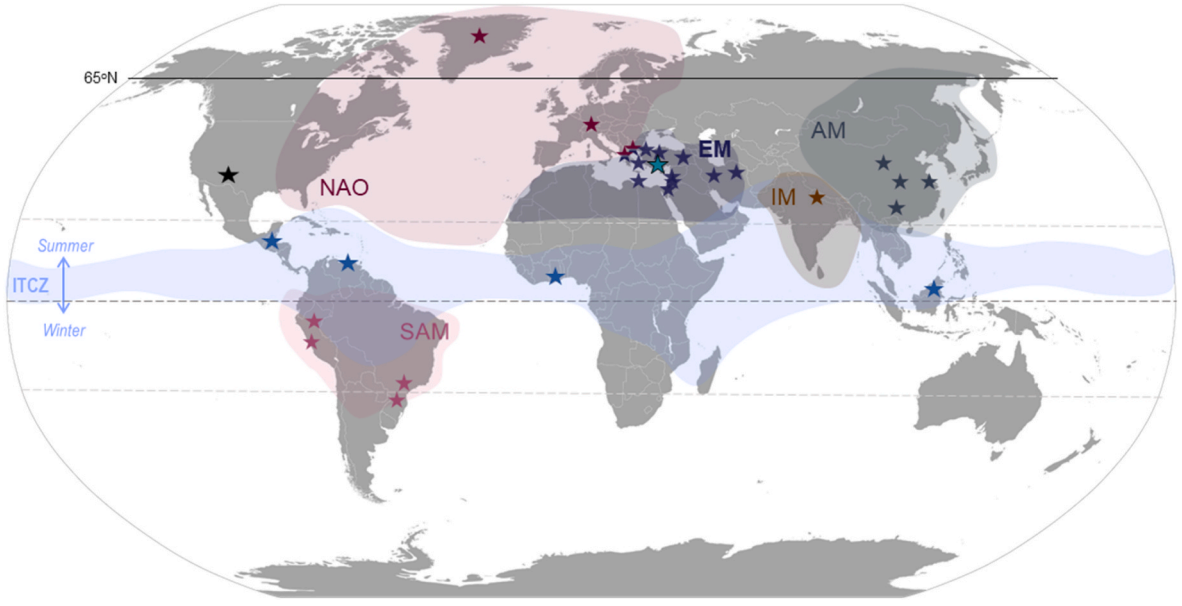

Fig. 1. Global distribution of major climate domains on Earth directly relevant to this study. Stars denote the locations of paleoclimate records referenced in this study (details in Table S1). Also shown are seasonal boundaries of ITCZ migration adapted from Deplazes et al.(Deplazes et al., 2013), with dashed lines marking the equator (dark grey), and tropics of Cancer and Capricorn (light grey). The location of Dim Cave is marked as a larger teal star.

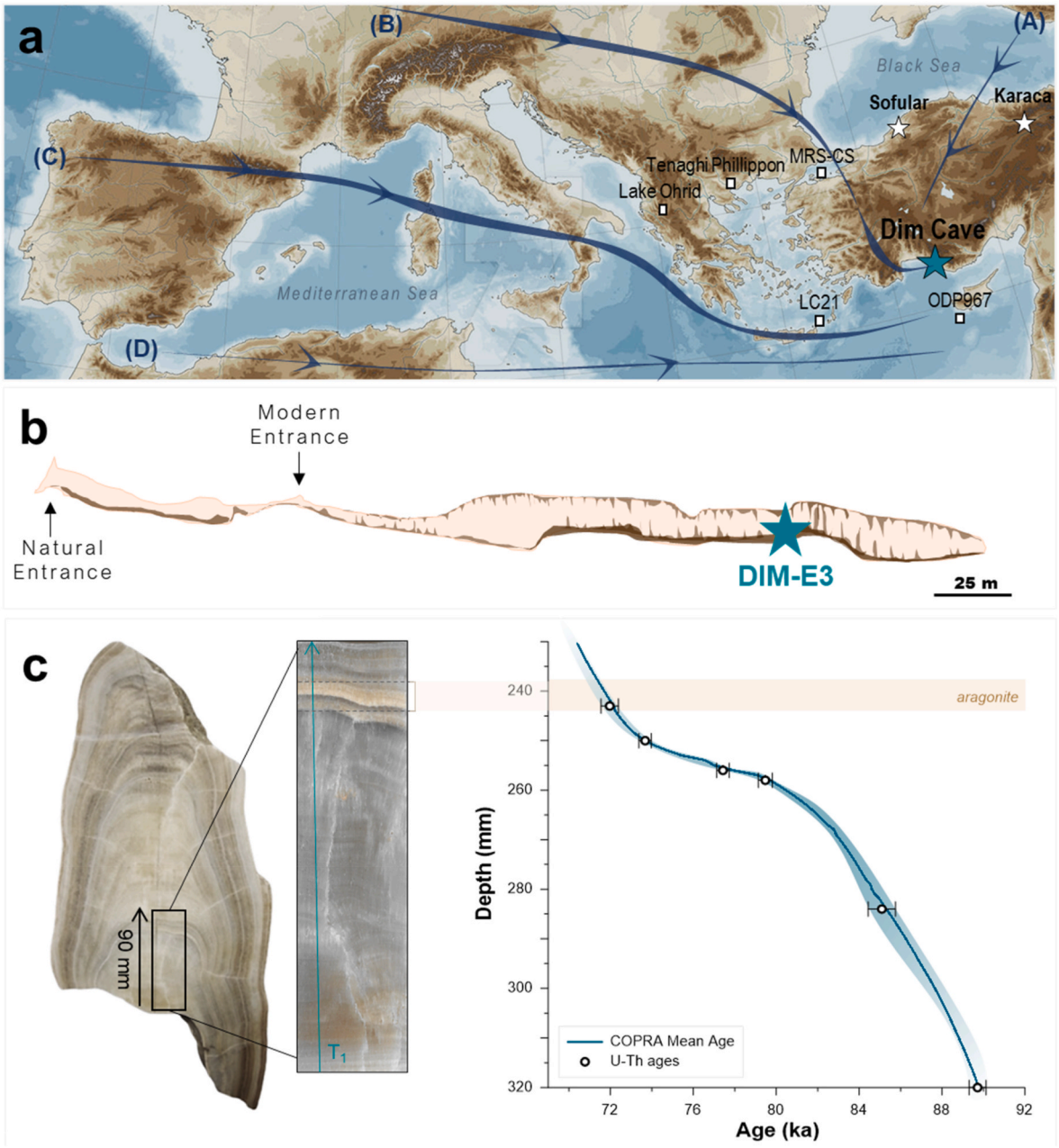

Fig. 2. **(a)** Relief map of the Mediterranean basin, with the location of Dim Cave (Alanya; southern Türkiye) marked as a teal star. Blue arrows mark four primary air mass tracks. All exert a measurable influence on the climate of the Eastern Mediterranean, but vary in moisture content and temperature, and hence rainwater isotope composition: (A) a NE-SW trajectory coming from Russia, Caucasus and modified in the Eastern Mediterranean region by transit over the Black Sea, (B) a NW-SE European trajectory across the Balkans; (C) a W-E Mediterranean (or North African coastal) trajectory where the air mass passes over the sea; (D) an inland African trajectory travelling SW-NE (adapted from Ünal-İmer et al.(Ünal-Imer et al., 2015)). The Dim Cave site is affected predominantly by tracks by (2) and (3), due to the shelter provided by the Central Taurus Mountains, separating the southern Türkiye from the central plateau (Ünal-Imer et al., 2015). **(b)** Projected profile of Dim Cave re-drawn and simplified from an archived report of the General Directorate of Mineral Research and Exploration (Türkiye) (Gündalı, 1989). The growth location of the DIM-E3 stalagmite is marked as a teal star. **(c)** Photograph of the stalagmite (DIM-E3) analysed here with a box showing the 90 mm long sub-sample DIM-E3-A analysed in this study (320-230 mm from the stalagmite tip). Also shown is the age-depth model for DIM-E3-A used in this study, where black circles mark U–Th age data (2σ uncertainties given as vertical bars). Teal shading marks 95% confidence intervals for the COPRA model age-depth interpolation (computed after Comas-Bru et al., 2020)).

ratio analysis of this stalagmite covering the last glacial period (~90–13 ka) revealed oscillations in $\delta^{18}O$ and $\delta^{13}C$ interpreted as reflecting millennial-scale latitudinal changes in the trajectories of westerly air masses over the Eastern Mediterranean, their associated moisture sources, and effects on ecosystem structure (Ünal-Imer et al., 2015, 2016). This study explores the extent to which the trace element composition of this stalagmite provides information regarding the timing, expression, and magnitude of climate variability across the MIS 5-to-4 transition (~90–70 ka) to ascertain how the global-scale climate shifts documented across this transition affected the Eastern Mediterranean.

2. Methods

2.1. Site & sample description

Dim Cave (also known as Gavurini Cave) is situated at 36°32′N, 32°06′E, 232 m above sea level in the Southern Dim River Valley (Central Taurus Mountains) within the upper Alanya geological unit-Yumrudağ Nappe (Okay and Özgül, 1984). The cave itself is comprised of grey-dark grey, early Triassic faulted and recrystallized dolomitic limestone (Gündalı, 1989). The cave is overlain by thin, nutrient-poor, and water deficient soils. Regional vegetation is composed of mostly red pine and scrubs (C3 type) typically found in Mediterranean climate zones. The cave has a simple morphology consisting of a single main horizontal passage ~360 m long and 10–15 m wide, terminating at a small (~200 m^2) subterranean lake on a bed of impermeable schist (Fig. 2a) (Ünal-Imer et al., 2015). Relative humidity in the cave is >90% and the temperature is 18–19°C, which is directly comparable to mean annual temperatures recorded at the coastal station of Antalya, 130 km WNW of Dim Cave and 50m above sea level (18.4°C; 1963–2004) (Rowe et al., 2020). The area is characterized by a typical Mediterranean climate, with warm to hot, dry summers and mild to cool, wet winters, and a mean annual temperature of ~18°C.

Cave drip and pool water samples suggest that winter precipitation is the dominant source of cave moisture, and that the stalagmite was fed by well-mixed seepage flow (Ünal-Imer et al., 2015). This is consistent with data recorded by the local meteorological station in Antalya Province, which shows that the region receives >70% of its annual rainfall (~1100 mm) between November and February, and ~98% between October and May. During a recent monitoring study, a sharp cave CO_2 reduction occurred in mid-August 2018 (Fig. S2) broadly coinciding with a rainfall increase marking the start of autumn weather patterns. These measurements suggest that cave air CO_2 is probably driven by seasonal shifts in cave versus outside air temperature, with cold (low CO_2) outside air flooding into the site when external temperatures drop below cave air temperatures (Baldini et al., 2006; James et al., 2015). Dim Cave is richly decorated with speleothems, from which production of several high-resolution stable oxygen and carbon isotope records have provided detailed information on past climatic and environmental conditions in Southern Türkiye during the penultimate and last glacial cycle: Dim-1 (~132–128 ka; Rowe et al., 2020), DIM-E2 (~13–10 ka), DIM-E3 (~89–13 ka) and DIM-E4 (~14.5–12 ka) (Ünal-Imer et al., 2015, 2016).

In this study we focus on stalagmite DIM-E3, which was collected from Dim Cave in June 2012, ~250 m from the natural cave entrance (Fig. 2b). Following collection the stalagmite was halved using a circular saw, with one half micro-sampled along the growth axis for U-series dating, stable isotope ($\delta^{18}O$ and $\delta^{13}C$), and wet ICP-MS trace element analyses at the University of Queensland (full analytical procedures reported in Ünal-Imer et al. (2015). The resulting chronology suggests that DIM-E3 grew continuously between 89.7 ± 0.4 and 13.3 ± 0.3 (2σ) ka. Growth rates peaked at ~11.9 mm/kyr, with two periods of distinctly slower growth also noted between ~72 and 63 ka and ~40–18 ka (~0.8 mm/kyr) (Table S2) (Ünal-Imer et al., 2016). In general, columnar fabric in calcite implies competitive growth with occasional breaks at crystal boundaries (or interfaces) and slow but constant drip rates, whereas open and elongated types of columnar fabric indicate faster flow (Frisia, 2015). Textural analysis of DIM-E3 confirms that growth fabric of this stalagmite predominantly reflects water availability in the Dim Cave throughout the last glacial period (~90–11 ka) (Ünal-Imer et al., 2016).

DIM-E3 consists predominantly of columnar calcite (C), alternating between elongated columnar (Ce) columnar open (Co) fabrics (*coding in* Frisia, 2015). The speleothem also contains several thin but clearly defined aragonite layers between 245 and 230 mm depth (Fig. 2b–S2). These layers are present as distinct bands spanning the width of the sample, with sharp boundaries visible between the calcite and aragonite structures fabrics (Ünal-Imer et al., 2016). The aragonite layers are also identifiable by pronounced peaks in strontium (Sr), barium (Ba), and uranium (U), owing to the orthorhombic crystal structure of aragonite that preferentially incorporates larger cations relative to smaller cations such as magnesium (Mg) (Wassenburg et al., 2016). These ionic size differences cause considerable differences in the distribution coefficients of the calcite and aragonite sections (Domínguez-Villar et al., 2017; He et al., 2021; Jamieson et al., 2016), complicating the interpretation of the geochemical signals in terms of hydroclimate. Thus, trace element measurements corresponding to the short aragonite-dominated sections of DIM-E3-A are not included in presentation and interpretation of the trace element profiles, but the presence of aragonite across these intervals is considered as an important petrographic feature with paleoclimate implications.

2.2. LA-ICP-MS

We analysed the lower 90 mm of the DIM-E3 stalagmite (320-230 mm below the tip; termed DIM-E3-A; Fig. 2c–S2) for seventeen trace elements at a 10 μm resolution (rectangular track). Sample track 1 (T_1) was analysed at Institut für Geowissenschaften, Goethe Universität (Germany). T_1 constitutes the longest track and was taken along the principal growth axis of the stalagmite, such that the path direction of the laser track was always perpendicular to the individual stalagmite laminae. Trace elements were measured using a prototype RESO-lution M-50 excimer laser-ablation system (193 nm), in conjunction with a two-volume laser-ablation cell, coupled to an Agilent 7500 ce/cs quadrupole ICP-MS. A 90 mJ laser spot with an estimated average diameter of 74 μm was used, with a 10 μm/s scan speed and a 15 Hz repetition rate following the methodology described in (Müller et al., 2009).

To assess the lateral consistency of the geochemical signals recorded in T_1, geochemical profiles for track T_1 were compared with a second, parallel track (T_2) taken slightly off-axis but adjacent to T_1. Data for T_2 were obtained at the Department of Earth Sciences, Durham University, using a Teledyne Analyte Excite+ 193 nm laser ablation system, with a two-volume laser-ablation cell coupled to a Thermo iCap TQe (QQQ-ICP-MS). A 10 × 150 μm laser slit allowed for sampling of a wide track, thus maximizing elemental precision but without compromising spatial resolution along the growth direction of the speleothem. The main analysis track was run on exactly the same position as the pre-ablation track at a 10 Hz repetition rate, 10 μm/s scan speed, and depth of 5 mm. Both analyses were bracketed by analyses of NIST 612, NIST 610, and MACS3 standards, and ^{43}Ca was measured as an internal standard. Data reduction was done manually using a rolling average of 0.63 μm, which translated to a temporal resolution of ~0.02-kyr per data point. Full analytical descriptions for both T_1 and T_2 are provided in the **Supplementary Methods**. Comparison of magnesium (Mg) profiles obtained for tracks T_1 and T_2 show broad agreement, with subtle offsets likely explained by geochemical variability as a function of distance from the principal growth axis (Fig. S4). This agreement suggests that the low-frequency variability recorded in T_1 reflects geochemical changes that contiguous across the DIM-E3-A stalagmite; the T_1 track forms the basis of our interpretations herein.

2.3. Chronology

U–Th ages and stable isotope measurements (2σ) are summarized in Table S2. Methodological details on geochronology and isotope analyses were reported in Ünal-Imer et al. (2016, 2015). Here we use these U–Th ages, their 2σ uncertainties, and the COPRA (Breitenbach et al., 2012) algorithm to produce an age model for DIM-E3-A (Fig. 2c). Our model yields ages of 89.7 ± 0.4 (2σ) ka for the base of the sample (320 mm below the stalagmite tip) and 70.6 ± 0.3 (2σ) ka for the top (230 mm below the stalagmite tip), which are consistent with the linear chronology presented by (Ünal-Imer et al., 2015). Trace element

measurements were assigned to a time axis by converting the spatial distance along T_1 converted to a time axis using COPRA (Fig. 2).

2.4. Principal component analysis

To explore variability in the DIM-E3-A trace element record, a principal component analysis (PCA) was performed on the T_1 dataset. PCA combines the intra-variable association, data dispersion direction, and relative importance of these directions to assess which principal component (PC) explains the largest sum of variability (Abdi and Williams, 2010). Applying this approach to speleothem compositional data can quantify the relationships between all measured elements, rather than focusing on single element profiles or element/element ratios. Therefore, it permits exploration of compositional changes across a continuous sequence, providing valuable constraints on the timing and nature of these changes, and thus their associated environmental signals (Baldini et al., 2015; Jamieson et al., 2015; Klaes et al., 2022; Stockhecke et al., 2016).

3. Results & Discussion

3.1. Controls on stalagmite geochemistry

Stalagmite DIM-E3 grew in a chamber ~150 m from the modern cave entrance (Fig. 2), and environmental monitoring suggests that site is removed from direct external temperature influences. Quantifying the correlations present between individual elements allows identification of the dominant influences on drip water composition, and the extent to which these can be related to the dolomitic limestone in which the cave is formed (Fig. 3, S4; Table S5). Clear groupings of trace elements exist; for example, strong positive correlations exist between elements highly compatible with calcite such as Mg, Sr, and Ba, terrigenous elements such as Nd, Y, La, and Cd, and organic colloid-associated elements such as P and Co. Perhaps unsurprisingly, the most significant negative correlations are typically observed between elements classified in different groups of the periodic table (e.g., Mg and P, $r^2 = -0.28$) (Fig. 3).

The PCA confirms the presence of distinct variability in the trace element composition of DIM-E3-A, but also reveals changes in the significance of different elements through time (Fig. 4). The first three principal components account for ~50% of variance in the dataset. Positive values of the leading principal component (PC1; 19.6 %) are dominated by the rare-earth elements (Y, Nd, La), with elements Cu, Cd, Zn, Yb, and U often associated with detrital material also making significant contributions (>0.25). Element loadings for PC2 (18.1 %) are dominated by calcite-compatible elements Mg, Sr, and Ba, and PC3 (11.4 %) by P and Co, both commonly associated with organic colloids (Figs. S3 and S4).

Principal Component 1 (PC1) (19.6%) is dominated by elements not typically incorporated into calcite (with some exceptions), and so we interpret this component as an indicator of detrital mineral fluxes into the Dim Cave. Elements Cd, Rb, Yb, U, and the REEs are commonly hosted in bedrock and surficial soils, and so heavily influenced by the intensity of both erosion and weathering above the cave (Ayalon et al., 1999; Frumkin and Stein, 2004; Zhou et al., 2008a). For example, relatively high U loading values in both PC1 (0.32) and PC2 (0.21) (Table S5) may indicate that several environmental processes influenced the mobilization, transport, and deposition of this element in the Dim Cave system. Indeed, dynamic changes in surface run-off, aeolian forces, and soil degradation can increase the mobilization and transport of detrital elements into sub-terrain karst systems as colloidal and particulate phases in drip waters (Hartland et al., 2012; Sliwinski et al., 2023), causing them to be deposited onto stalagmites either as visible layers of mud/silt (Zhornyak et al., 2011), or as microscopic particles concentrated in individual calcite layers (Klaes et al., 2022; Paine et al., 2021a); as is the case for DIM-E3-A. Hence, the presence (or absence) of detrital elements in a stalagmite record can signal changes in the rate and

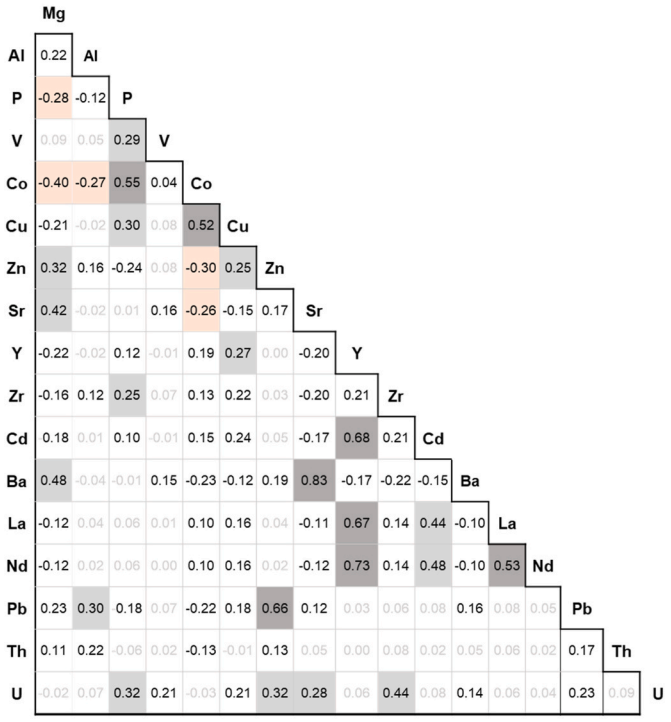

BEDROCK COMPOSITION

Element	Concentration (ppm)	%
Mg	125.5	35.1
P	0.6	0.2
Ca	230.3	64.5
Fe	0.6	0.2
Sr	0.06	0.02

Fig. 3. Correlation matrix for trace elements measured using LA-ICPMS in the DIM-E3 Transect #1. Values given are Pearson correlation coefficients (r) to indicate the direction and strength of the association between two elements, where r = −1 represents a perfect negative association, r = 0 represents no association, and r = 1 represents a perfect positive association. Grey shading indicates positive correlations (light: >0.25, dark: >0.5), and orange shading indicates negative correlations (light: <-0.25, dark: <-0.5) at 99% significance ($p < 0.01$). Thus, higher values suggest that similar processes influenced the concentration of the two elements in tandem. Values between 0.1 and −0.1 are greyed-out for clarity. Inset table provides the concentration of dominant cations for the dolomitic limestone hosting the Dim Cave (first presented in Ünal-Imer et al. (2016)). Elements presented are those displaying contributions to this composition >0.001 %.

intensity of dynamic processes affecting the surficial environment (Borsato et al., 2007; Fairchild and Treble, 2009).

High PC1 values are concentrated within three distinct intervals: ~90–87 ka, ~85–81 ka, and ~73.5–70 ka (Fig. 5). The timing of these peaks corresponds to distinctly different hydrological conditions, suggesting they may also record different environmental processes. For example, the two intervals corresponding to high PC1 scores prior to ~80 ka also correspond to a more elongated columnar calcite structure, which would favour incorporation of relatively insoluble phases and/or ligands (Pearson et al., 2020; Sliwinski et al., 2023) (Fig. 5). Low and relatively stable $\delta^{18}O$ and $\delta^{13}C$ values (Ünal-Imer et al., 2015) coinciding with the high PC1 scores imply consistently high moisture availability at the site prior to ~81 ka; likely in the form of precipitation. Frequent precipitation events would enhance surface run-off processes, more intense soil and bedrock weathering, and subsequently increase the detrital flux to the stalagmite as a function of increased flow energy (Borsato et al., 2007; Hartland et al., 2012; Tan et al., 2014; Zhou et al., 2008a, 2008b, 2012). Conversely, the PC1 increase between ~73.5 and 70 ka corresponds to several high-amplitude fluctuations in $\delta^{13}C$, pertaining to dynamic climate conditions less favorable for consistent

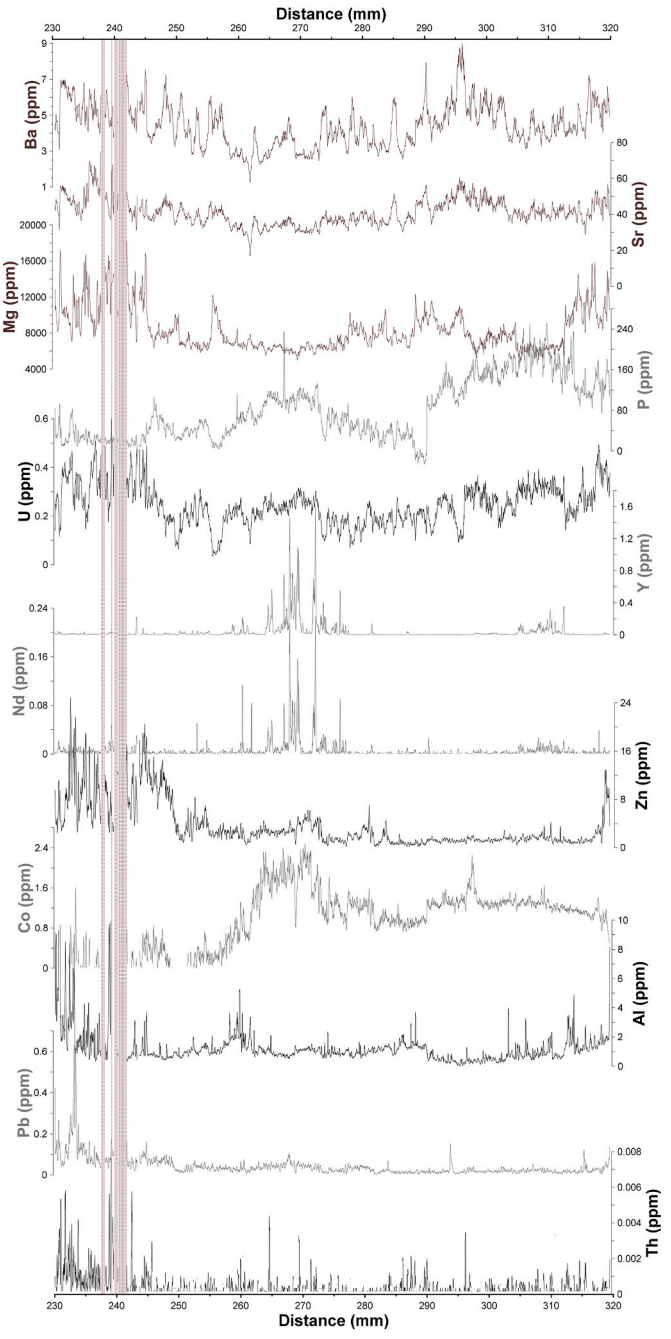

Fig. 4. Trace element data generated by, and analysed in, this study. The stalagmite is dominantly calcite in composition, but it also possesses several clearly defined aragonite layers at between 245 and 230 mm depth (brown shading). Because uncertainty regarding the exact distribution coefficients of the calcite and aragonite exist, we have opted to not present the trace element data from aragonitic sections of DIM-E3-A here. However, we do consider the mineralogical differences in our interpretations, and include a figure showing trace element profiles corresponding to these sections in Figure S5 (*supplementary file*).

vegetation growth and development of stable soil structures (Ünal-Imer et al., 2015). Sparsely vegetated soils are more prone to being weathered by wind and water (Regattieri et al., 2016), suggesting that detrital elements were more readily mobilized and transported into the Dim Cave system during seasonal heavy rainfall events across this time interval.

Principal Component 2 (PC2) (18.1%) comprises the bedrock-sourced alkaline earth elements Mg, Sr, and Ba. Variations in these three trace elements typically record bedrock contributions to drip water chemistry, with enrichments signalling enhanced bedrock dissolution, and lower overall moisture availability (Fairchild et al., 2000; Fairchild and Treble, 2009; Stoll et al., 2012; Wassenburg et al., 2020). Drier conditions would increase the ground water residence time in the aquifer prior to deposition at the stalagmite growth site, facilitating higher rates of limestone dissolution, degassing from the precipitating waters, and prior calcite precipitation (PCP) (Sherwin and Baldini, 2011; Wassenburg et al., 2020). Agreement between the known and modelled Mg/Sr relationship for this stalagmite suggests that PCP affected Mg, Sr, and Ba concentrations in DIM-E3-A (Fig. 6). Higher PC2 scores therefore suggest stronger interactions between the Dim Cave drip waters and bedrock and reduced effective recharge, but the strength of this process was not necessarily linear through time.

Elevated PC2 values occur between ~90 and 86 ka, and ~79–70 ka (Fig. 5). Given that PCP typically increases as effective recharge decreases (Domínguez-Villar et al., 2017; Fairchild and McMillan, 2007; McMillan et al., 2005; Wassenburg et al., 2012), elevated PC2 scores suggest reduced rainfall across these intervals. However, high PC2 scores are not always synchronous with the higher PC1 and PC3 values, highlighting differences in trace element transport processes between the two aforementioned intervals. For example, peaks in PC2 between ~90 and 86 ka coincide with high PC1 and PC3 scores and only a modest increase in $\delta^{18}O$ and $\delta^{13}C$ values, potentially associated with high moisture supply and soil activity (Ünal-Imer et al., 2015). Conversely, decoupling between PC2, PC1, and PC3 occurs in the ~79 and 70 ka interval (Fig. 5), when peaks in PC2 correspond to persistently low PC3 scores (<0; Fig. 5), and the increase in PC1 lags ~5.5-kyr behind the PC2 series (Fig. 5).

The highest PC2 scores are concentrated between ~73.8 and 70 ka, coinciding with greater variability in $\delta^{18}O$ (changing moisture sources; Ünal-Imer et al., 2015), more compact calcite fabrics (slow growth rates), and culminating in recurrent aragonite deposition (Ünal-Imer et al., 2016). All pertain to distinctly lower moisture availability in the cave, causing elevated rates of PCP and subsequent enrichment of drip waters in Mg, Sr, and Ba (Fig. 4). The PCP process affects the balance between drip water Mg/Ca, Sr/Ca, and Ba/Ca ratio, drip water pH, and calcite saturation index, meaning that all three generally become elevated during periods of low moisture availability (He et al., 2021; Wassenburg et al., 2020). Hence, calcite-aragonite transitions are often interpreted as aridity indicators, on the basis that reduced effective precipitation results in decreased water flow through the karst (e.g., McMillan et al., 2005). The suggestion that PCP is tightly coupled to moisture availability in Dim Cave is supported by evidence for PC2 peaks in DIM-E3-A corresponding to evidence for drier conditions both within and outside the cave (Fig. 5), but also minima corresponding to evidence for wetter conditions. For example, the lowest PC2 scores between ~86 and 79 ka corresponding to the highest PC1 scores (Fig. 5), pronounced reductions in $\delta^{18}O$ and $\delta^{13}C$ (Ünal-Imer et al., 2015), and elongated columnar fabrics pertaining to accelerated stalagmite growth (Ünal-Imer et al., 2016), suggesting that elevated moisture availability served to preclude (or at least minimise) PCP-related effects on drip waters during climatic intervals characterised by elevated precipitation and soil activity.

Principal Component 3 (PC3) (11.4 %) is dominated by soluble elements phosphorus (P) and cobalt (Co). Speleothem P derives principally from the leaching of decomposing organic matter in the soil, and is readily transported by pH-neutral groundwaters (Borsato et al., 2007; Treble et al., 2003). Prior studies have interpreted speleothem P as a proxy for bioproductivity of the overlying soils at the time of deposition, with higher P concentrations linked to elevated primary productivity, water infiltration, and colloidal transport (Baldini et al., 2002; Fairchild et al., 2001; Regattieri et al., 2016). Less is known about the behavior of Co in calcite (Fairchild and Treble, 2009), however the presence of a strong correlation with P in this record could suggest a common transport process. The bioavailability of Co is similarly higher in acidic, vegetated, thick soils (Srivastava et al., 2022), suggesting this element

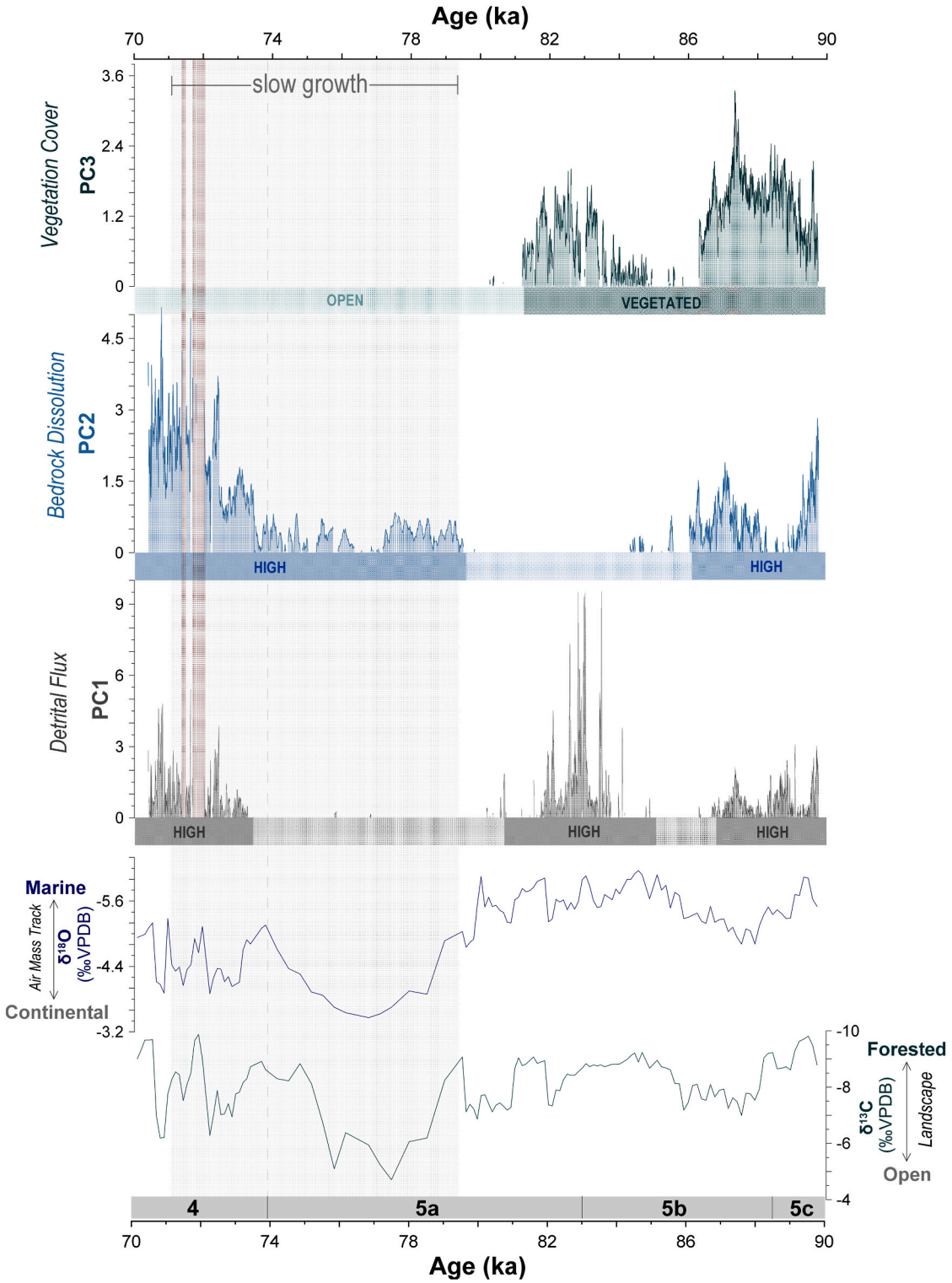

Fig. 5. PCA scores from the DIM-E3-A trace element dataset, presented as a function of time. PC1 is dominated by poorly soluble elements typically transported into caves in particle and colloidal form, suggesting that this component reflects changes in detrital input. PC2 comprises the alkaline earth elements known to signal prior-calcite-precipitation, suggesting this component reflects shifts in the strength of cave water-bedrock interactions (see main text and **supplementary file**). Finally, PC3 is dominated by soluble elements typically transported in colloidal/solute form and thus allude to enhanced soil weathering and high bioproductivity. Time series' shown for each principal component are an 8-point moving arithmetic mean. Horizontal grey shading shows an interval of slower stalagmite growth based on evidence for more closed/compressed columnar fabrics, and enhanced water-rock interactions indicative of longer water residence times (Ünal-Imer et al., 2016). Brown shading shows calcite-aragonite transitions in DIM-E3-A consistent with covariation of Ba, Sr, U, and Mg spikes; the stalagmite is entirely calcite outside of this age range. $\delta^{18}O$, and $\delta^{13}C$ data from the same stalagmite section are also presented (Ünal-Imer et al., 2015), and grey bars at the bottom of the figure denote chronostratigraphic boundaries of glacial succession in Eastern Europe (Hughes et al., 2022), labelled based on their corresponding Marine Isotope Stage (Lisiecki and Raymo, 2005).

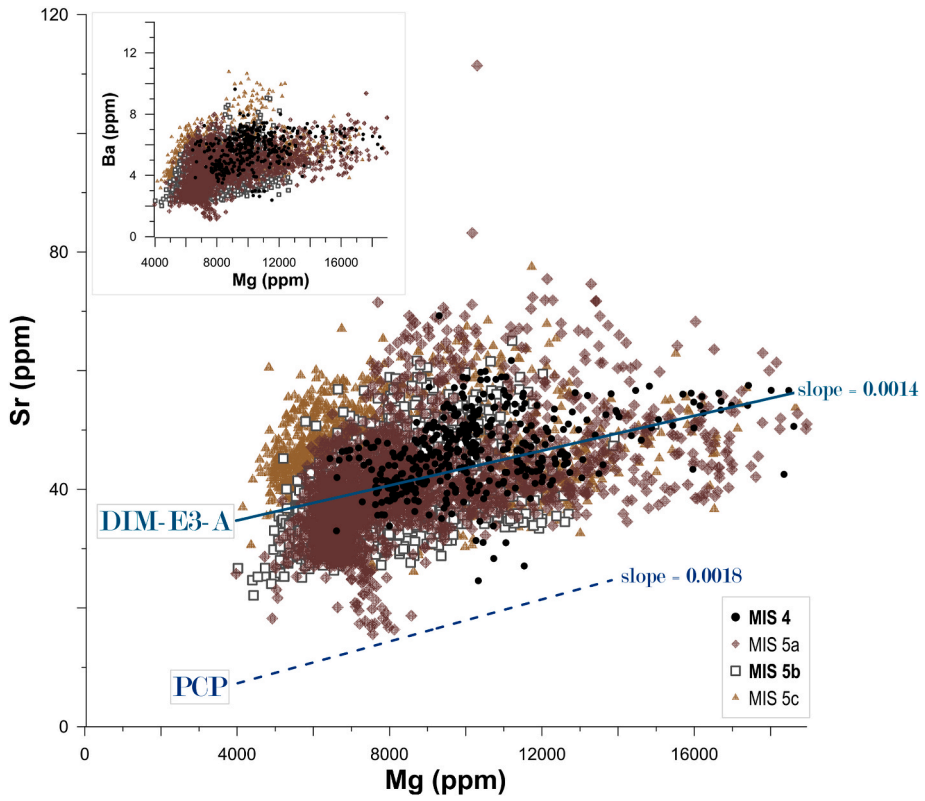

Fig. 6. Relationship between Mg and Sr in DIM-E3-A between ~90 and 70 ka, presented in parts per million (ppm). Line 'PCP' shows the theoretical slope modelled for prior calcite precipitation (see **Text S4**). Colour and shape coding marks data values corresponding to key climate intervals between ~90 and 70 ka (based on the chronostratigraphy for Southern Europe presented by Hughes et al.(Hughes et al., 2022)). ***Inset graph*:** relationship between Mg and Ba. If partition coefficients of Mg, Sr, and Ba are assumed to be constant, then speleothems forming under the influence of PCP are expected to display a positive linear correlation between these three elements. Our data gives a slope of 0.0014 for the Mg/Sr relationship. Given the similarity of this value to the PCP-modelled slope, this suggests that PCP is a strong candidate for the mechanism responsible for the observed correlations seen in DIM-E3-A between ~90 and 70 ka.

may be more readily mobilized through binding to organic matter in a manner similar to trace metals such as copper (Cu) (Borsato et al., 2007) and mercury (Hg) (Ravichandran, 2004). This bioavailability may be further enhanced by the local geology, as the Dim Cave bedrock is known to be predominantly dolomitic limestone (Ünal-Imer et al., 2016): rock types rich in iron (Fe) and manganese (Mn), and both with high capacity to adsorb both divalent and trivalent Co cations in surface soils (Kosiorek and Wyszkowski, 2019; Medyńska-Juraszek et al., 2020; Perez-Espinosa et al., 2005; Srivastava et al., 2022).

Elevated PC3 scores in DIM-E3-A are concentrated between ~90 and 81 ka (Fig. 5). Low $\delta^{18}O$ and $\delta^{13}C$ values and high speleothem growth rates both suggest more humid conditions during this interval, favorable for good vegetation and soil development (Ünal-Imer et al., 2015), and effective mobilization of organic-bound trace elements. Hence, these elements would likely be more susceptible to transport into the cave by surface runoff. Less clear is what prompted a sudden drop in PC3 (<0) observed between ~86.5 and 85 ka, which also corresponds to simultaneous reductions in PC1 and PC2 (Fig. 5). A coeval increase $\delta^{13}C$ could signal a transient reduction in terrestrial bioproductivity due to colder and/or drier conditions; perhaps related to Greenland Stadial-21.2 as recorded in high-latitude ice cores, or simply due to local-scale variability in ambient temperature, hydrology, and/or biological processes (Ünal-Imer et al., 2015).

3.2. Marine Isotope Stages 5c and 5b

Climate conditions recorded in DIM-E3-A during MIS 5c (~96–87 ka) and 5b (~87–82 ka) are characterised by wet and warm conditions (Fig. 5). Peaks in PC1 and PC3 point to high influx of detrital and organic-bound minerals, resulting from more intense pluvial (precipitation-driven) erosion and mobilization of trace elements preferentially transported as mineral particles and/or bound to organic colloids from the soils (Borsato et al., 2007; Fairchild and Treble, 2009; Hartland et al., 2012). A concurrent reduction in water residence time (PC2) and low $\delta^{13}C$ values supports this interpretation by signaling frequent groundwater recharge, and forest expansion in the catchment (Ünal-Imer et al., 2015, 2016), respectively. Furthermore, weakening of the Mg/Sr relationship relative to predicted values suggests an additional Mg/Sr supply to the stalagmite (Fig. 6), potentially by increased recharge of the aquifer above the cave. Particularly large peaks in PC1 and PC3 suggest this 'flushing' process was particularly strong between ~84 and 81 ka (Fig. 5).

Climate variability during MIS 5c and 5b revealed by the new DIM-E3-A trace element dataset appear comparable to other paleoclimate records from the Eastern Mediterranean (Fig. 7). For example, reduced $\delta^{18}O$ and/or $\delta^{13}C$ in speleothems extracted from Soreq, Pequiin (Israel; Bar-Matthews et al., 2003; 1997)), Qal'e Kord, Pir Ghar (Iran; Carolin et al., 2019; Mehterian et al., 2017)), Sofular (Türkiye; Held et al., 2024), and Wintimdouine (Morocco; Ait Brahim et al., 2023)) caves correspond to peaks in calcium ion supply to lakes Ohrid (Macedonia; Wagner et al., 2019) and Yammouneh (Lebanon; Gasse et al., 2015)), and evidence for rapid forest expansion in the Eastern Mediterranean (Litt et al., 2014; Pickarski et al., 2015), the Levant (Miebach et al., 2019), the Balkans (Donders et al., 2021; Koutsodendris et al., 2023; Sadori et al., 2016), and North Africa (Lézine et al., 2019; Miller et al., 2016) – all signaling high moisture availability throughout MIS 5c and 5b (Fig. 7). The effects of this increase within the Dim Cave catchment would be an increase total surface run-off, flushing large quantities of detrital matter/coarse colloids from the overlying soils into the cave, increasing hydraulic weathering of the Mg-rich bedrock, and reductions

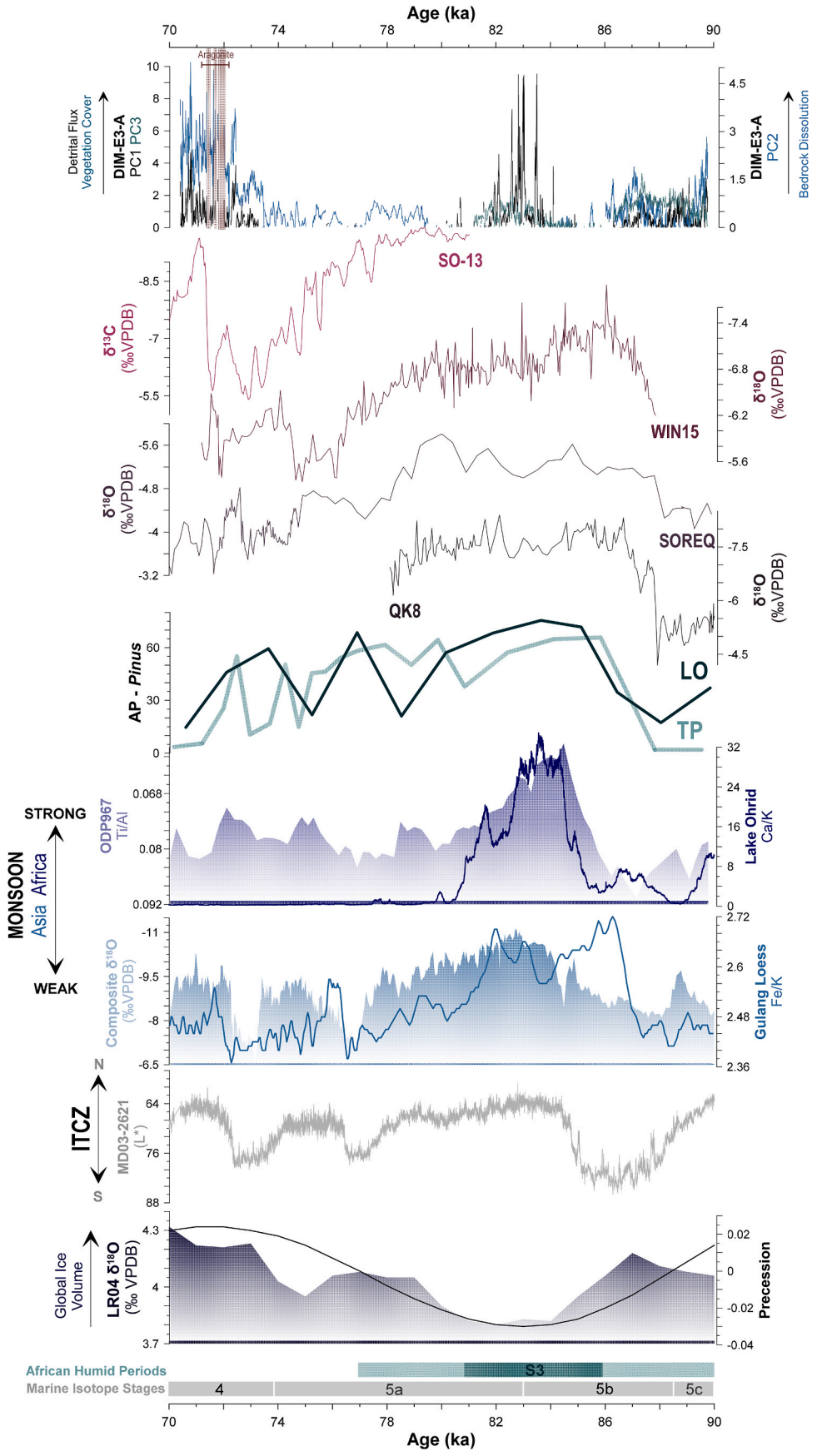

(caption on next page)

Fig. 7. Variations in PC1, PC2, and PC3 scores for the DIM-E3-A, compared with high-resolution northern hemisphere paleoclimate records spanning the ~90–70 ka interval. These records are as follows: $\delta^{18}O$ profiles from Soreq (Israel; Bar-Matthews et al., 1997), Qal'e Kord (Iran; Mehterian et al., 2017), and Wintimdouine (Morocco; Ait Brahim et al., 2023) caves, a $\delta^{13}C$ profile from Sofular Cave (Turkey; Held et al., 2024), a composite speleothem $\delta^{18}O$ record from China (Cheng et al., 2016), sedimentary Ca/K ratios from Lake Ohrid (Macedonia/Albania; Wagner et al., 2019)), arboreal pollen excluding Pinus (AP-*Pinus*) from Tenaghi Phillippon (TP) (Greece; Koutsodendris et al., 2023) and Lake Ohrid (LO) (Macedonia/Albania; (Donders et al., 2021), Ti/Al ratios recorded in Ocean Drilling Project (ODP) site 967 (Eastern Mediterranean; Grant et al., 2022; 2017), Fe/K ratios recorded in the Gulang loess sequence (China; Sun et al., 2021), sediment total reflectance (L*, sm200) in marine core MD03-26 from offshore South America (Cariaco Basin, Venezuela; Deplazes et al., 2013), a time series of Earth's precessional index (Berger and Loutre, 1991), and a composite marine $\delta^{18}O$ stack as a record of global ice volume (LR04; Lisiecki and Raymo, 2005)). Further details for each of the archives included in this figure are provided in Table S1. Light grey boxes denote chronostratigraphic boundaries of glacial succession in Eastern Europe (Hughes et al., 2022), labelled based on their corresponding Marine Isotope Stage. A pale green box marks African Humid Period 3 – an interval corresponding to evidence for northward migration of the tropical rain belt, covering large areas of North Africa with river systems, lakes, and dense vegetation and resulting in large sediment influxes to the Mediterranean Basin (Ehrmann and Schmiedl, 2021). A dark green box denotes the timing of sapropel 3 (S3) formation relative to this period. Brown vertical shading shows calcite-aragonite transitions in DIM-E3-A.

in dissolution and PCP-related processes (Figs. 5 and 7).

Detrital and organic influxes (PC1 & PC3) peak in DIM-E3-A between 83.5 ± 0.3 (2σ) and 81.9 ± 0.3 (2σ) ka (Fig. 5). This signal directly corresponds to evidence for intensification of precipitation across the Eastern Mediterranean culminating in formation of sapropel 3 (S3) (Fig. 7). Sapropels form in response to increased flux of freshwater to the Mediterranean basin via the Nile and wider North African channel network, and closely correspond to variability in Earth's orbital precession cycle (Rohling et al., 2015). Low precession increases both summer insolation (NHSI) maxima and winter insolation (NHWI) minima in the northern hemisphere (Barker et al., 2011; Sun et al., 2021; Wagner et al., 2019), driving northward displacement, narrowing, and intensification of ITCZ-modulated precipitation, and NH Hadley cell positioning (Asmerom et al., 2020; Deplazes et al., 2013). By amplifying the persistence of high-pressure systems, sea surface temperatures, and convection over the Mediterranean Sea, this displacement produces a stronger African monsoon, surface-water freshening and reduced deep-water ventilation (Fig. 7). The ensuing S3 signal (~86–81 ka) is recorded in marine sediment records from both the Mediterranean (Grant et al., 2022, 2016; Rohling et al., 2015) and Sea of Marmara (Çağatay et al., 2019) and directly corresponds to evidence for heightened influx of detrital matter (PC1) in DIM-E3-A, but also more abundant vegetation in the catchment (PC3) (Fig. 5). The latter signal suggests this geochemical variability was produced by an increase in the frequency and intensity of local precipitation, resulting in heightened pluvial erosion, transport, and infiltration of detrital materials into the cave, while also fueling a more productive terrestrial ecosystem.

3.3. Marine Isotope Stages 5a to 4 (~81–70 ka)

Trace element variability in DIM-E3-A changes distinctly during MIS 5a (~78–75 ka). Unlike the detrital (PC1) signals recorded during MIS 5c and 5b, higher values recorded from ~81 ka instead coincide with low PC3 and moderate PC2 scores (Fig. 5). These trace element shifts also correspond to a notable increase in $\delta^{18}O$ and $\delta^{13}C$ values (Fig. 5; Ünal-Imer et al., 2015), an increase in calcite density (Ünal-Imer et al., 2016), and strengthening of the Mg/Sr relationship relative to modelled values (Fig. S8); each indicative of a reduction in moisture availability both within and outside the Dim Cave, slowdown of stalagmite growth, and increased groundwater residence times. Whereas the PC2 signal during MIS 5a may reflect a steady increase in PCP, the low PC3 values suggest higher erosion rates, surface weathering, and soil thinning (Ünal-Imer et al., 2015). These processes would reduce the soil's capacity for retention of detrital elements, enhancing the mobilization and transport of these elements into the cave by surface runoff, while simultaneously diluting fluxes of organic matter into the karst system (Borsato et al., 2007; Fairchild and Treble, 2009; Hartland et al., 2012). Coinciding with these trace element changes are also clear increases in both $\delta^{18}O$ and $\delta^{13}C$ (Ünal-Imer et al., 2015). Both suggest a shift toward drier conditions in southern Türkiye during MIS 5a: an interpretation supported by coupled trace element and isotope variations indicative of drier, more arid conditions in the Dim-1 stalagmite across the penultimate glacial – interglacial transition (Fig. S1; Rowe et al., 2020).

Aridity-driven geochemical variability intensifies in DIM-E3-A at ~74 ka (Fig. 5). Sharp peaks in PC2 scores are accompanied by increased concentrations of exotic trace elements within DIM-E3-A's mineral fabric, such as Zn, U, and Pb (Fig. 4), while $\delta^{18}O$ values remain high (Fig. 5). These high values are followed by sporadic aragonite growth between ~72.3 and 71.3 ka, and clear peaks in Mg, Ba, and Sr immediately prior to the first calcite-to-aragonite transformation suggests these result from increased interactions between host rock and seepage waters, elevated rates of bedrock dissolution, and simultaneous calcite precipitation from the water leading to an enrichment in fluid Mg/Ca. Given that the factors driving such transformations (e.g., balance between drip water Mg/Ca, Sr/Ca, and Ba/Ca ratio) must surpass a given threshold before aragonite deposition can occur (Wassenburg et al., 2012), this implies that moisture availability decreased substantially after 74 ka and that aridity peaked in ~72.3 ka in the Eastern Mediterranean. Calcite-to-aragonite transitions are also not present in DIM-E3 after ~71.3 ka (Ünal-Imer et al., 2016), which implies that the hydroclimatic conditions favouring this geochemical variability in DIM-E3-A did not occur again following the MIS 5-to-4 transition.

Severely arid conditions in the Eastern Mediterranean across the MIS 5-to-4 transition are consistently recorded in paleoclimate archives across the region as precipitation reductions and/or increased continental dust flux (Fig. 7). Speleothem $\delta^{18}O$ profiles (Bar-Matthews et al., 1997, 2003; Carolin et al., 2019; Mehterian et al., 2017), and lacustrine/peat-based pollen reconstructions (Donders et al., 2021; Koutsodendris et al., 2023; Litt et al., 2014; Miebach et al., 2019; Panagiotopoulos et al., 2014; Pickarski et al., 2015; Sadori et al., 2016) suggest simultaneous reductions in precipitation, atmospheric humidity, and surface temperatures starting at ~80 ka, with distinct minima concentrated between ~74 and 72 ka (Fig. 7). Several terrestrial lakes also record pronounced increased sedimentation rates produced by the release of eroded materials stored in lake beds, river beds, and soils during earlier stages of MIS 5, often in response to fluctuations in lake level and precipitation/evaporation balance (Stockhecke et al., 2016; Wagner et al., 2014). Combined with transient model simulations, all attest to increasing orbital precession as the driver of these changes via Northern Hemisphere Summer Insolation (NHSI) reductions (Kutzbach et al., 2014; Stockhecke et al., 2016; Zhang et al., 2021), decreasing sea and land surface temperatures (Wagner et al., 2019), expansion and southward displacement of the ITCZ (Deplazes et al., 2013), reduced convection over the Mediterranean, and subsequent weakening of African monsoon (Grant et al., 2017; Wagner et al., 2019) (Fig. 7).

Aridity in the Eastern Mediterranean between ~81 and ~70 ka was also associated with increased regional dust fluxes (Ehrmann and Schmiedl, 2021; Grant et al., 2017). Changing atmospheric pressure gradients over the Mediterranean basin would have produced stronger westerly winds (Wagner et al., 2019), with advection of cold and dry continental air from the Balkans directly toward the Eastern Mediterranean (Fig. 7; Ünal-Imer et al. (2015). Stronger winds would have increased the atmospheric dust load, and this evidence for wind strengthening also corresponds to increased dust fluxes into this region

from North Africa (Ben-Israel et al., 2015; Ehrmann et al., 2017; Gross et al., 2016; Vaks et al., 2010) and/or Central Europe (Újvári et al., 2010). Although stronger winds and increased dust fluxes are not always contemporaneous with increased aridity (and vice versa), these signals clearly correspond to evidence for widespread reductions in moisture availability, such as vegetation thinning in the Dim Cave catchment (Fig. 4; Ünal-Imer et al., 2015), and forest recession across the Mediterranean (Koutsodendris et al., 2023; Panagiotopoulos et al., 2014). Both suggest a decrease in effective precipitation coupled with an increase in soil instability and exposure, suggesting that peaks in PC1 scores in DIM-E3-A during MIS 4 could also capture an increase in aeolian dust flux to the site in response to stronger westerly winds (Verniers et al., 2022), and heightened erosion of these exposed soils.

Clear deviation of the Mg/Sr relationship from a modelled PCP vector during MIS 4 further supports our interpretation that the geochemical variability in DIM-E3-A following ~74 ka reflects heightened aridity (Fig. S8). This deviation also corresponds to clear peaks in Th concentration and identification of the highest $^{87}Sr/^{86}Sr$ ratios in

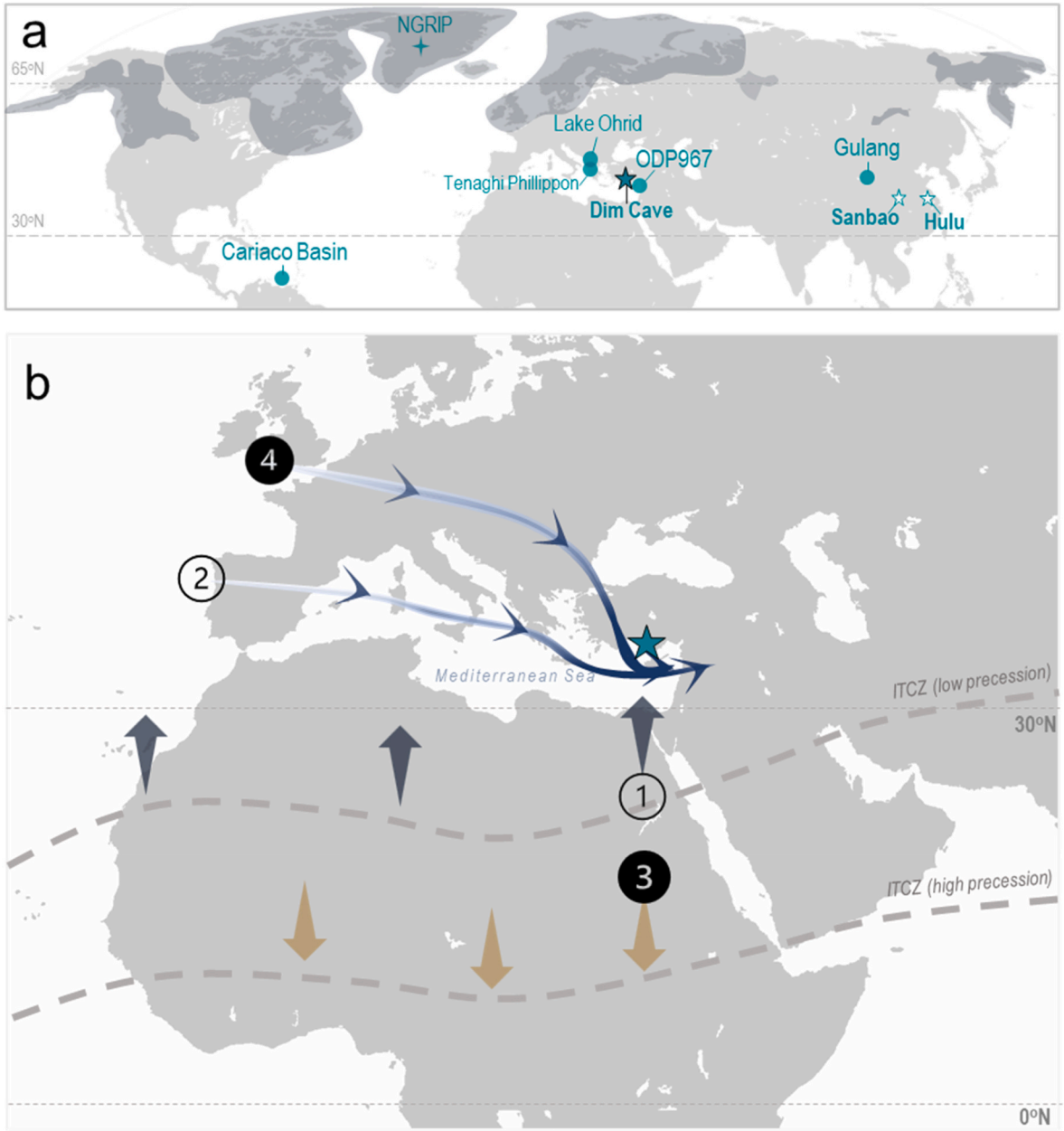

Fig. 8. **(a)** A map of the Northern Hemisphere, where Dim Cave is labelled as a teal star, and dark blue shading marks maximum NH ice sheet extents corresponding to our interval of interest (reconstructed by Batchelor et al. (2019)). The locations of Lake Ohrid, Tenaghi Phillippon, site ODP967, Hulu cave, Sanbao Cave, the Gulang loess site, the Cariaco Basin, and the NGRIP drill site are also displayed. **(b)** A schematic representation of hydroclimatic changes in the Eastern Mediterranean between ~90 and 70 ka. Two paleoclimatic intervals are described and marked, with numbers denoting key features of each interval, respectively. ***MIS 5c to 5b*** (~90–81 ka; transparent circles): (1) low orbital precession drives intensification of African monsoon, causing northward displacement of the ITCZ and NH Hadley cells during summer, and increased precipitation in the Eastern Mediterranean; (2) westerly winds travel on a predominantly a W-E Mediterranean trajectory where the air masses pass predominantly over the Mediterranean sea, minimizing continental dust uptake and increasing overall atmospheric moisture; ***MIS 5a to 4*** (~81–70 ka; filled circles): (3) increasing precession during MIS 5a results in progressive weakening of the African Monsoon which, in conjunction with growing NH ice sheets (e.g., panel **(a)**), pushes the ITCZ southward to reduce precipitation in the EM; (4) westerly winds shift to follow a continental, NW-SE European trajectory across the Balkans which, coupled with reduced vegetation cover (low moisture availability) and increased wind activity, enhances erosion and aeolian transport of dust over the EM. In conjunction with mechanism (3), this signal culminates in the rapid transition to strong glacial conditions during MIS 4.

DIM-E3 during MIS 4 (Fig. S8; Ünal-Imer et al., 2016), which could also reflect increased influence of atmospheric dust on the composition of these drip waters. Following deposition in soils above the cave, these dust particles would be mobilized by erosion, and more readily transported to the karst aquifer by seasonal precipitation due to thinning of terrestrial vegetation caused by colder, drier conditions (Ünal-Imer et al., 2015).

3.4. Global teleconnections

Combining trace element data from DIM-E3-A with Mediterranean paleoclimate data across the MIS 5-to-4 transition reveals a climate shift faster, and more severe, than any similar transition during the last glacial. This severity is also documented across the northern hemisphere. For example, a pronounced isotope excursion in the North Greenland Ice Core (NGRIP) record at 74.1 ± 0.06 ka (known as Greenland Stadial-20 (GS-20) (Rasmussen et al., 2014)) suggests a rapid (<300 years) reduction in temperature (>10°C), and increase in atmospheric dust content (Fig. S9; Kindler et al., 2014; Rasmussen et al., 2014). This high-latitude signal is synchronous with $\delta^{18}O$ excursions indicative of anomalously weak (dry) monsoon events in stalagmite records from Asia (Cheng et al., 2016; Du et al., 2019; Wang et al., 2001) and India (Kathayat et al., 2016), and drought events in the southwestern USA (Polyak et al., 2017) and Borneo (Carolin et al., 2013). Several lake sediment records also document abrupt changes in water level (Baxter et al., 2023; Brooks et al., 2005; Mueller et al., 2010; Scholz et al., 2007; Stockhecke et al., 2016; Wagner et al., 2014; Waldmann et al., 2009), and/or pollen concentrations (Camuera et al., 2019; Kern et al., 2022; Lézine et al., 2019; Scholz et al., 2007). In the Southern Hemisphere, the timing of MIS 4 initiation corresponds to a progressive rise in Antarctic temperature (Capron et al., 2010; EPICA Project Members, 2006), and distinct increases in precipitation recorded in $\delta^{18}O$ archives from Botuverá (Cruz et al., 2005; Wang et al., 2006) and Cueva del Diamante (Cheng et al., 2013) caves (Brazil). The global-scale synchronicity of this signal suggests that the unique conditions driving its occurrence were exclusive to the end of MIS 5, underscoring the pervasive nature of coupled ocean-atmosphere-cryosphere interactions during the last glacial (Brook and Buizert, 2018; EPICA Project Members, 2006). Hence, this suggests that strong, global-scale forcing mechanisms likely underpinned the centennial-scale environmental changes recorded in DIM-E3-A, and indeed across the Eastern Mediterranean (Fig. 8).

DIM-E3-A also provides a climatic context for understanding hominin dispersal patterns. Proxy and model-based evidence suggest that the relatively stable, humid conditions of MIS 5c and 5b provided opportune corridors for hominin dispersal across Northeast Africa (e.g., Fischer et al., 2024; Foerster et al., 2022; Schaebitz et al., 2021) and Southwest Asia (e.g., Abbas et al., 2023; Bae et al., 2017; Barzilai et al., 2022; Groucutt et al., 2018, 2021). However, the rate of drying and environmental stress documented in this speleothem ($<10^2$-year timescales) across the MIS 5a-to-4 transition would have been too rapid to trigger distinct physiological adaptations or even mass relocation – particularly in a geographically discontinuous and physiologically-demanding region such as the Eastern Mediterranean (Zittis et al., 2022). Therefore, responses to increased climatological stress may instead have taken the form of changes in social behaviour (e.g., collaboration), technological innovation, and occupation of higher-altitude sites to escape hyper-arid conditions in the lowlands (Fischer et al., 2024).

The fundamental question of why the MIS 5-to-4 transition was so distinct remains unresolved. Reductions in high-latitude insolation have been linked to decreased sea-surface temperatures and subsequent expansion of sea-ice cover in the subpolar North Atlantic, with effects including diminished North Atlantic Deep Water (NADW) formation, weakening of the Atlantic meridional overturning circulation (AMOC), and a southward ITCZ shift (Fig. 7) (Henry et al., 2016; Zhang et al., 2021). On one hand, the positive feedbacks instigated by these processes could have both amplified and sustained the cooling that occurred during this transition(Li and Born, 2019; Menviel et al., 2020), with strong teleconnections facilitating the southward propagation of the resulting climate perturbations into the Eastern Mediterranean (Bar-Matthews et al., 2003; Mehterian et al., 2017). However, the models employed to test these feedbacks still cannot reproduce climate variability with comparable characteristics to those observed in proxy records (Li and Born, 2019), precluding the ability to establish whether the ocean and atmospheric circulation changes that took place prior to/during the MIS 5-to-4 transition were a cause, or effect (Lynch-Stieglitz, 2017).

Five high-magnitude (M), radiometrically dated volcanic eruptions also show intriguing proximity to the onset of MIS 4, and subsequently the anomalously severe climate excursions described above (Fig. S10). These five eruptions are the M9.1 eruption of Toba volcano, Indonesia at 73.9 ± 0.3 (1σ) ka (Storey et al., 2012), the M8.1 eruption of Atitlán volcano, Guatemala 75 ± 2 (1σ) ka (Cisneros de León et al., 2021), the M6.6 eruption of Valles Caldera, New Mexico at 74.4 ± 1.3 (2σ) ka (Zimmerer et al., 2016), a couplet of M6.6 and M6 eruptions of Coatepeque caldera at 72 ± 3(2σ) ka (Kutterolf et al., 2020), and the M6 eruption of Mount Mazama at 71 ± 5(1σ) ka (Bacon and Lanphere, 2006). Studies have suggested that dynamical, systemic responses to volcanic aerosol forcing could result in long-lasting (>10-yr) effects on sea ice expansion, deep ocean convection, atmospheric circulation (Colose et al., 2016; Erez and Adam, 2021; Ridley et al., 2015), and AMOC strength (Miller et al., 2012; Slawinska and Robock, 2018; Zhong et al., 2011); with consequences measurable far from the eruptive source. However, the idea that volcanism could trigger millennia-scale climate change has received comparatively little research attention due to chronological uncertainties and the incompleteness of the Quaternary eruption record (Baldini et al., 2015; Crosweller et al., 2012; Paine et al., 2021b). Although the severity of the MIS 5-to-4 transition cannot be conclusively linked to volcanic forcing, improvements in last glacial eruption dating, cohesion between geological and chemostratigraphic eruption records, and modelling of long-term volcanic impacts on the climate system will allow for further exploration of this hypothesis (Paine et al., 2021b).

4. Conclusions

The shift from Marine Isotope Stage (MIS) 5 to 4 is distinct among interglacial-glacial transitions within the last glacial period. Focusing on the trace element composition of a stalagmite from Dim Cave (south Türkiye), our study sheds light on two distinct climatic signals corresponding to this shift in the Eastern Mediterranean. First is a pronounced increase in moisture availability between MIS 5c and 5b (~90–81 ka), which is indicated by a higher influx of detrital and organic-bound elements to the growing stalagmite. This influx is attributed to intensified precipitation-driven erosion, frequent groundwater recharge, low water-bedrock interaction, and expansion of the forest cover in the catchment area: a signal which peaks in conjunction with the onset of sapropel 3 (S3) in the Mediterranean region. The second signal occurs across the MIS 5a to MIS 4 transition (~81–70 ka), where elevated influx of detrital elements coupled with increased rates of bedrock dissolution, erosion, surface weathering, soil thinning, and a progressive mineralogical change in DIM-E3-A suggests low moisture availability both within and outside the cave. This aridity-driven signal peaks after ~74 ka, corresponding to an unusually rapid shift to severe cold and dry conditions recorded in paleoclimate records across the northern hemisphere. By assessing the DIM-E3-A trace element data relative to the signals captured by existing paleoclimate archives, orbitally driven oscillations in African monsoon strength and position present a mechanistic explanation for the hydroclimatic signals recorded in our stalagmite across the MIS 5-to-4 transition, and suggest that global-scale hydroclimate shifts could swiftly and extensively impact the environment in the Eastern Mediterranean on timescales ranging from decades

to millennia. Not only do our findings underscore the potential environmental consequences of abrupt climate change in the future, but they also emphasize how speleothem trace element records can shed crucial light on the timing, expression, and magnitude of climate variability during the last glacial period.

Author contributions

ARP – conceptualization, formal analysis, methodology, investigation, writing (original draft); JULB – conceptualization, methodology; EÜİ – conceptualization, resources; FBW – conceptualization; AAI – methodology, investigation, data curation; MCSH – methodology, data curation; RJB – conceptualization, WM– methodology, investigation; CO – methodology. All authors contributed to manuscript preparation.

Declaration of competing interest

The authors declare that they have no known competing financial interests or personal relationships that could have appeared to influence the work reported in this paper.

Data availability

Data will be made available on request.

Acknowledgments

All authors greatly thank Dr. Fuat Şaroğlu and operating manager Murat Ünal of MAĞ-TUR Dim Cave Establishment for permission to study Dim Cave speleothems, Tom Verniers, and Dr Stacy Carolin for valuable inputs to study conceptualization. ARP acknowledges funding from European Research Council Consolidator Grant V-ECHO (ERC-2018-COG-8187 17-V-ECHO). Thanks must also go to Julian Andrews and a second anonymous reviewer for their contributions to peer review of this work, and whose feedback inspired significant improvements to the study.

Appendix A. Supplementary Information

Supplementary information to this article can be found online at https://doi.org/10.1016/j.quascirev.2024.108841.

References

Abbas, M., Lai, Z., Jansen, J.D., Tu, H., Alqudah, M., Xu, X., Al-Saqarat, B.S., Al Hseinat, M., Ou, X., Petraglia, M.D., Carling, P.A., 2023. Human dispersals out of Africa via the levant. Sci. Adv. 9, eadi6838 https://doi.org/10.1126/sciadv.adi6838.

Abdi, H., Williams, L.J., 2010. Principal component analysis. Wiley Interdisciplinary Reviews: Comput. Stat. 2, 433–459.

Ait Brahim, Y., Sha, L., Wassenburg, J.A., Azennoud, K., Cheng, H., Cruz, F.W., Bouchaou, L., 2023. The spatiotemporal extent of the Green Sahara during the last glacial period. iScience 26, 107018. https://doi.org/10.1016/j.isci.2023.107018.

Asmerom, Y., Baldini, J.U.L., Prufer, K.M., Polyak, V.J., Ridley, H.E., Aquino, V.V., Baldini, L.M., Breitenbach, S.F.M., Macpherson, C.G., Kennett, D.J., 2020. Intertropical convergence zone variability in the neotropics during the common era. Sci. Adv. 6, 1–8. https://doi.org/10.1126/sciadv.aax3644.

Ayalon, A., Bar-Matthews, M., Kaufman, A., 1999. Petrography, strontium, barium and uranium concentrations, and strontium and uranium isotope ratios in speleothems as palaeoclimatic proxies: Soreq Cave, Israel. Holocene 9, 715–722. https://doi.org/10.1191/095968399673664163.

Bacon, C.R., Lanphere, L.A., 2006. Eruptive history and geochronology of Mount Mazama and the crater lake region, Oregon. Geol. Soc. Am. Bull. 118, 1331–1359.

Bae, C.J., Douka, K., Petraglia, M.D., 2017. On the origin of modern humans: Asian perspectives. Science 358, eaai9067. https://doi.org/10.1126/science.aai9067.

Baldini, J.U.L., Baldini, L.M., McDermott, F., Clipson, N., 2006. Carbon dioxide sources, sinks, and spatial variability in shallow temperate zone caves: evidence from Ballynamintra cave, Ireland. J. Cave Karst Stud. 68, 4–11.

Baldini, J.U.L., Brown, R.J., McElwaine, J.N., 2015. Was millennial scale climate change during the Last Glacial triggered by explosive volcanism? Sci. Rep. 5, 1–9. https://doi.org/10.1038/srep17442.

Baldini, J.U.L., McDermott, F., Fairchild, I.J., 2002. Structure of the 8200-year cold event revealed by a speleothem trace element record. Science 296, 2203–2206. https://doi.org/10.1126/science.1071776.

Baldini, L.M., McDermott, F., Baldini, J.U.L., Arias, P., Cueto, M., Fairchild, I.J., Hoffmann, D.L., Mattey, D.P., Müller, W., Constantin Nita, D., Ontañón, R., Garciá-Moncó, C., Richards, D.A., 2015. Regional temperature, atmospheric circulation, and sea-ice variability within the Younger Dryas Event constrained using a speleothem from northern Iberia. Earth Planet Sci. Lett. 419, 101–110.

Barker, S., Knorr, G., Edwards, R.L., Parrenin, Frédéric, Putnam, A.E., Skinner, L.C., Wolff, E., Ziegler, M., Barker, S., Knorr, G., Edwards, R.L., Parrenin, Frederic, Putnam, A.E., Skinner, L.C., Wolff, E., Ziegler, M., 2011. 800 , 000 Years of abrupt climate variability. Science 334, 347–351.

Bar-Matthews, M., Ayalon, A., Gilmour, M., Matthews, A., Hawkesworth, C.J., 2003. Sea - land oxygen isotopic relationships from planktonic foraminifera and speleothems in the Eastern Mediterranean region and their implication for paleorainfall during interglacial intervals. Geochem. Cosmochim. Acta 67, 3181–3199. https://doi.org/10.1016/S0016-7037(02)01031-1.

Bar-Matthews, M., Ayalon, A., Kaufman, A., 1997. Late quaternary paleoclimate in the eastern mediterranean region from stable isotope analysis of speleothems at Soreq cave, Israel. Quat. res. 47, 155–168. https://doi.org/10.1006/qres.1997.1883.

Bar-Matthews, M., Keinan, J., Ayalon, A., 2019. Hydro-climate research of the late quaternary of the Eastern Mediterranean-Levant region based on speleothems research – a review. Quat. Sci. Rev. 221, 105872 https://doi.org/10.1016/j.quascirev.2019.105872.

Barzilai, O., Oron, M., Porat, N., White, D., Timms, R., Blockley, S., Zular, A., Avni, Y., Faershtein, G., Weiner, S., Boaretto, E., 2022. Expansion of eastern Mediterranean Middle Paleolithic into the desert region in early marine isotopic stage 5. Sci. Rep. 12, 4466. https://doi.org/10.1038/s41598-022-08296-9.

Batchelor, C.L., Margold, M., Krapp, M., Murton, D.K., Dalton, A.S., Gibbard, P.L., Stokes, C.R., Murton, J.B., Manica, A., 2019. The configuration of Northern Hemisphere ice sheets through the Quaternary. Nat. Commun. 10, 1–10. https://doi.org/10.1038/s41467-019-11601-2.

Baxter, A.J., Verschuren, D., Peterse, F., Miralles, D.G., Martin-Jones, C.M., Maitituerdi, A., Van Der Meeren, T., Van Daele, M., Lane, C.S., Haug, G.H., Olago, D. O., Sinninghe Damsté, J.S., 2023. Reversed holocene temperature–moisture relationship in the horn of Africa. Nature 620, 336–343. https://doi.org/10.1038/s41586-023-06272-5.

Ben-Israel, M., Enzel, Y., Amit, R., Erel, Y., 2015. Provenance of the various grain-size fractions in the negev loess and potential changes in major dust sources to the eastern mediterranean. Quat. res. 83, 105–115. https://doi.org/10.1016/j.yqres.2014.08.001.

Berger, A., Loutre, M.F., 1991. Insolation values for the climate of the last 10 million years. Quat. Sci. Rev. 10, 297–317. https://doi.org/10.1016/0277-3791(91)90033-Q.

Bergström, A., Stringer, C., Hajdinjak, M., Scerri, E.M.L., Skoglund, P., 2021. Origins of modern human ancestry. Nature 590, 229–237. https://doi.org/10.1038/s41586-021-03244-5.

Beyer, R.M., Krapp, M., Eriksson, A., Manica, A., 2021. Climatic windows for human migration out of Africa in the past 300,000 years. Nat. Commun. 12, 4889. https://doi.org/10.1038/s41467-021-24779-1.

Borsato, A., Frisia, S., Fairchild, I.J., Somogyi, A., Susini, J., 2007. Trace element distribution in annual stalagmite laminae mapped by micrometer-resolution X-ray fluorescence: implications for incorporation of environmentally significant species. Geochem. Cosmochim. Acta 71, 1494–1512. https://doi.org/10.1016/j.gca.2006.12.016.

Bradley, R.S., Diaz, H.F., 2021. Late quaternary abrupt climate change in the tropics and sub-tropics: the continental signal of tropical hydroclimatic events (THEs). Rev. Geophys. 59, e2020RG000732 https://doi.org/10.1029/2020RG000732.

Breitenbach, S.F.M., Rehfeld, K., Goswami, B., Baldini, J.U.L., Ridley, H.E., Kennett, D.J., Prufer, K.M., Aquino, V.V., Asmerom, Y., Polyak, V.J., Cheng, H., Kurths, J., Marwan, N., 2012. Constructing proxy records from age models (COPRA). Clim. Past 8, 1765–1779. https://doi.org/10.5194/cp-8-1765-2012.

Brook, E.J., Buizert, C., 2018. Antarctic and global climate history viewed from ice cores. Nature 558, 200–208. https://doi.org/10.1038/s41586-018-0172-5.

Brooks, K., Scholz, C.A., King, J.W., Peck, J., Overpeck, J.T., Russell, J.M., Amoako, P.Y. O., 2005. Late-Quaternary lowstands of lake Bosumtwi, Ghana: evidence from high-resolution seismic-reflection and sediment-core data. Palaeogeogr. Palaeoclimatol. Palaeoecol. 216, 235–249. https://doi.org/10.1016/j.palaeo.2004.10.005.

Çağatay, M.N., Eriş, K.K., Makaroğlu, Ö., Yakupoğlu, N., Henry, P., Leroy, S.A.G., Uçarkuş, G., Sakınç, M., Yalamaz, B., Bozyiğit, C., Kende, J., 2019. The Sea of Marmara during marine isotope stages 5 and 6. Quat. Sci. Rev. 220, 124–141. https://doi.org/10.1016/j.quascirev.2019.07.031.

Camuera, J., Jiménez-Moreno, G., Ramos-Román, M.J., García-Alix, A., Toney, J.L., Anderson, R.S., Jiménez-Espejo, F., Bright, J., Webster, C., Yanes, Y., Carrión, J.S., 2019. Vegetation and climate changes during the last two glacial-interglacial cycles in the western Mediterranean: a new long pollen record from Padul (southern Iberian Peninsula). Quat. Sci. Rev. 205, 86–105. https://doi.org/10.1016/j.quascirev.2018.12.013.

Camuera, J., Ramos-Román, M.J., Jiménez-Moreno, G., García-Alix, A., Ilvonen, L., Ruha, L., Gil-Romera, G., González-Sampériz, P., Seppä, H., 2022. Past 200 kyr hydroclimate variability in the western mediterranean and its connection to the african humid periods. Sci. Rep. 12, 1–13. https://doi.org/10.1038/s41598-022-12047-1.

Capron, E., Landais, A., Lemieux-Dudon, B., Schilt, A., Masson-Delmotte, V., Buiron, D., Chappellaz, J., Dahl-Jensen, D., Johnsen, S., Leuenberger, M., Loulergue, L., Oerter, H., 2010. Synchronising EDML and NorthGRIP ice cores using δ18O of

atmospheric oxygen (δ18Oatm) and CH4 measurements over MIS5 (80–123 kyr). Quat. Sci. Rev. 29, 222–234. https://doi.org/10.1016/j.quascirev.2009.07.014.
Carolin, S.A., Cobb, K.M., Adkins, J.F., Clark, B., Conroy, J.L., Lejau, S., Malang, J., Tuen, A.A., 2013. Varied response of western Pacific hydrology to climate forcings over the last glacial period. Science 340, 1564–1566. https://doi.org/10.1126/science.1233797.
Carolin, S.A., Ersek, V., Roberts, W.H.G., Walker, R.T., Henderson, G.M., 2019. Drying in the Middle East during northern hemisphere cold events of the early glacial period. Geophys. Res. Lett. 46, 14003–14010. https://doi.org/10.1029/2019GL084365.
Cheng, H., Edwards, R.L., Sinha, A., Spötl, C., Yi, L., Chen, S., Kelly, M., Kathayat, G., Wang, X., Li, X., Kong, X., Wang, Y., Ning, Y., Zhang, H., 2016. The Asian monsoon over the past 640,000 years and ice age terminations. Nature 534, 640–646. https://doi.org/10.1038/nature18591.
Cheng, H., Sinha, A., Cruz, F.W., Wang, X., Edwards, R.L., D'Horta, F.M., Ribas, C.C., Vuille, M., Stott, L.D., Auler, A.S., 2013. Climate change patterns in Amazonia and biodiversity. Nat. Commun. 4, 1411. https://doi.org/10.1038/ncomms2415.
Cisneros de León, A., Schindlbeck-Belo, J.C., Kutterolf, S., Danišík, M., Schmitt, A.K., Freundt, A., Pérez, W., Harvey, J.C., Wang, K.L., Lee, H.Y., 2021. A history of violence: magma incubation, timing and tephra distribution of the Los Chocoyos supereruption (Atitlán Caldera, Guatemala). J. Quat. Sci. https://doi.org/10.1002/jqs.3265.
Colose, C.M., LeGrande, A.N., Vuille, M., 2016. Hemispherically asymmetric volcanic forcing of tropical hydroclimate during the last millennium. Earth System Dynamics 7, 681–696. https://doi.org/10.5194/esd-7-681-2016.
Comas-Bru, L., Atsawawaranunt, K., Harrison, S., S.W.G.M., 2020. SISAL (Speleothem Isotopes Synthesis and AnaLysis Working Group) Database Version 2.0. Database.
Crosweller, H.S., Arora, B., Brown, S.K., Cottrell, E., Deligne, N.I., Guerrero, N.O., Hobbs, L., Kiyosugi, K., Loughlin, S.C., Lowndes, J., Nayembil, M., Siebert, L., Sparks, R.S.J., Takarada, S., Venzke, E., 2012. Global database on large magnitude explosive volcanic eruptions (LaMEVE). Journal of Applied Volcanology 1, 1–13. https://doi.org/10.1186/2191-5040-1-4.
Cruz, F.W., Burns, S.J., Karmann, I., Sharp, W.D., Vuille, M., Cardoso, A.O., Ferrari, J.A., Silva Dias, P.L., Viana, O., 2005. Insolation-driven changes in atmospheric circulation over the past 116,000 years in subtropical Brazil. Nature 434, 63–66. https://doi.org/10.1029/2003jb002684.
Dai, A., 2013. Increasing drought under global warming in observations and models. Nat. Clim. Change 3, 52–58. https://doi.org/10.1038/nclimate1633.
Deplazes, G., Lückge, A., Peterson, L.C., Timmermann, A., Hamann, Y., Hughen, K.A., Röhl, U., Laj, C., Cane, M.A., Sigman, D.M., Haug, G.H., 2013. Links between tropical rainfall and North Atlantic climate during the last glacial period. Nat. Geosci. 6, 213–217. https://doi.org/10.1038/ngeo1712.
Domínguez-Villar, D., Krklec, K., Pelicon, P., Fairchild, I.J., Cheng, H., Edwards, L.R., 2017. Geochemistry of speleothems affected by aragonite to calcite recrystallization – potential inheritance from the precursor mineral. Geochem. Cosmochim. Acta 200, 310–329. https://doi.org/10.1016/j.gca.2016.11.040.
Donders, T., Panagiotopoulos, K., Koutsodendris, A., Bertini, A., Mercuri, A.M., Masi, A., Combourieu-Nebout, N., Joannin, S., Kouli, K., Kousis, I., Peyron, O., Torri, P., Florenzano, A., Francke, A., Wagner, B., Sadori, L., 2021. 1.36 million years of Mediterranean forest refugium dynamics in response to glacial-interglacial cycle strength. Proc. Natl. Acad. Sci. U.S.A. 118 https://doi.org/10.1073/pnas.2026111118.
Drysdale, R.N., Zanchetta, G., Hellstrom, J.C., Fallick, A.E., McDonald, J., Cartwright, I., 2007. Stalagmite evidence for the precise timing of North Atlantic cold events during the early last glacial. Geology 35, 77–80. https://doi.org/10.1130/G23161A.1.
Du, W., Cheng, H., Xu, Y., Yang, X., Zhang, P., Sha, L., Li, H., Zhu, X., Zhang, M., Stríkis, N.M., Cruz, F.W., Edwards, R.L., Zhang, H., Ning, Y., 2019. Timing and structure of the weak Asian Monsoon event about 73,000 years ago. Quat. Geochronol. 53, 101003 https://doi.org/10.1016/j.quageo.2019.05.002.
Ehrmann, W., Schmiedl, G., 2021. Nature and dynamics of North African humid and dry periods during the last 200,000 years documented in the clay fraction of eastern mediterranean deep-sea sediments. Quat. Sci. Rev. 260, 106925 https://doi.org/10.1016/j.quascirev.2021.106925.
Ehrmann, W., Schmiedl, G., Beuscher, S., Krüger, S., 2017. Intensity of african humid periods estimated from saharan dust fluxes. PLoS One 12, 1–18. https://doi.org/10.1371/journal.pone.0170989.
EPICA Project Members, 2006. One-to-one coupling of glacial climate variability in Greenland and Antarctica. Nature 444, 195–198.
Erez, M., Adam, O., 2021. Energetic constraints on the time-dependent response of the ITCZ to volcanic eruptions. J. Clim. 34, 9989–10006. https://doi.org/10.1175/JCLI-D-21-0146.1.
Fairchild, I.J., Baker, A., Borsato, A., Frisia, S., Hinton, R.W., McDermott, F., Tooth, A.F., 2001. High-resolution, multiple-trace-element variation in speleothems. J. Geol. Soc. 158, 831–841. London.
Fairchild, I.J., McMillan, E.A., 2007. Speleothems as indicators of wet and dry periods. Int. J. Speleol. 36, 69–74. https://doi.org/10.5038/1827-806X.36.2.2.
Fairchild, I.J., Smith, C.L., Baker, A., Fuller, L., Spotl, C., Mattey, D.P., McDermott, F., E, I.M.F., 2000. Controls on trace element (Sr-Mg) compositions of carbonate cave waters: implications for speleothem climatic records. Chem. Geol. 166, 255–269.
Fairchild, I.J., Treble, P.C., 2009. Trace elements in speleothems as recorders of environmental change. Quat. Sci. Rev. 28, 449–468. https://doi.org/10.1016/j.quascirev.2008.11.007.
Fischer, M.L., Munz, P.M., Asrat, A., Foerster, V., Kaboth-Bahr, S., Marwan, N., Schaebitz, F., Schwanghart, W., Trauth, M.H., 2024. Spatio-temporal variations of climate along possible African-Arabian routes of H. sapiens expansion. Quaternary Science Advances 14, 100174. https://doi.org/10.1016/j.qsa.2024.100174.
Fleitmann, D., Burns, S.J., Neff, U., Mangini, A., Matter, A., 2003. Changing moisture sources over the last 330,000 years in Northern Oman from fluid-inclusion evidence in speleothems. Quat. Res. 60, 223–232. https://doi.org/10.1016/S0033-5894(03)00086-3.
Fleitmann, D., Cheng, H., Badertscher, S., Edwards, R.L., Mudelsee, M., Göktürk, O.M., Fankhauser, A., Pickering, R., Raible, C.C., Matter, A., Kramers, J., Tüysüz, O., 2009. Timing and climatic impact of Greenland interstadials recorded in stalagmites from northern Turkey. Geophys. Res. Lett. 36, 1–5. https://doi.org/10.1029/2009GL040050.
Foerster, V., Asrat, A., Bronk Ramsey, C., Brown, E.T., Chapot, M.S., Deino, A., Duesing, W., Grove, M., Hahn, A., Junginger, A., Kaboth-Bahr, S., Lane, C.S., Opitz, S., Noren, A., Roberts, H.M., Stockhecke, M., Tiedemann, R., Vidal, C.M., Vogelsang, R., Cohen, A.S., Lamb, H.F., Schaebitz, F., Trauth, M.H., 2022. Pleistocene climate variability in eastern Africa influenced hominin evolution. Nat. Geosci. 15, 805–811. https://doi.org/10.1038/s41561-022-01032-y.
Frisia, S., 2015. Microstratigraphic logging of calcite fabrics in speleothems as tool for palaeoclimate studies. IJS 44.
Frumkin, A., Stein, M., 2004. The Sahara–East Mediterranean dust and climate connection revealed by strontium and uranium isotopes in a Jerusalem speleothem. Earth Planet Sci. Lett. 217, 451–464. https://doi.org/10.1016/S0012-821X(03)00589-2.
Gasse, F., Vidal, L., Van Campo, E., Demory, F., Develle, A.-L., Tachikawa, K., Elias, A., Bard, E., Garcia, M., Sonzogni, C., Thouveny, N., 2015. Hydroclimatic changes in northern Levant over the past 400,000 years. Quat. Sci. Rev. 111, 1–8. https://doi.org/10.1016/j.quascirev.2014.12.019.
Grant, K.M., Amarathunga, U., Amies, J.D., Hu, P., Qian, Y., Penny, T., Rodriguez-Sanz, L., Zhao, X., Heslop, D., Liebrand, D., Hennekam, R., Westerhold, T., Gilmore, S., Lourens, L.J., Roberts, A.P., Rohling, E.J., 2022. Organic carbon burial in Mediterranean sapropels intensified during Green Sahara Periods since 3.2 Myr ago. Commun Earth Environ 3, 11. https://doi.org/10.1038/s43247-021-00339-9.
Grant, K.M., Grimm, R., Mikolajewicz, U., Marino, G., Ziegler, M., Rohling, E.J., 2016. The timing of Mediterranean sapropel deposition relative to insolation, sea-level and African monsoon changes. Quat. Sci. Rev. 140, 125–141. https://doi.org/10.1016/j.quascirev.2016.03.026.
Grant, K.M., Rohling, E.J., Westerhold, T., Zabel, M., Heslop, D., Konijnendijk, T., Lourens, L., 2017. A 3 million year index for North African humidity/aridity and the implication of potential pan-African Humid periods. Quat. Sci. Rev. 171, 100–118. https://doi.org/10.1016/j.quascirev.2017.07.005.
Gross, A., Palchan, D., Krom, M.D., Angert, A., 2016. Elemental and isotopic composition of surface soils from key Saharan dust sources. Chem. Geol. 442, 54–61. https://doi.org/10.1016/j.chemgeo.2016.09.001.
Groucutt, H.S., Grün, R., Zalmout, I.A.S., Drake, N.A., Armitage, S.J., Candy, I., Clark-Wilson, R., Louys, J., Breeze, P.S., Duval, M., Buck, L.T., Kivell, T.L., Pomeroy, E., Stephens, N.B., Stock, J.T., Stewart, M., Price, G.J., Kinsley, L., Sung, W.W., Alsharekh, A., Al-Omari, A., Zahir, M., Memesh, A.M., Abdulshakoor, A.J., Al-Masari, A.M., Bahameem, A.A., Al Murayyi, K.M.S., Zahrani, B., Scerri, E.L.M., Petraglia, M.D., 2018. Homo sapiens in Arabia by 85,000 years ago. Nat Ecol Evol 2, 800–809. https://doi.org/10.1038/s41559-018-0518-2.
Groucutt, H.S., White, T.S., Scerri, E.M.L., Andrieux, E., Clark-Wilson, R., Breeze, P.S., Armitage, S.J., Stewart, M., Drake, N., Louys, J., Price, G.J., Duval, M., Parton, A., Candy, I., Carleton, W.C., Shipton, C., Jennings, R.P., Zahir, M., Blinkhorn, J., Blockley, S., Al-Omari, A., Alsharekh, A.M., Petraglia, M.D., 2021. Multiple hominin dispersals into Southwest Asia over the past 400,000 years. Nature 597, 376–380. https://doi.org/10.1038/s41586-021-03863-y.
Gündalı, N., 1989. Dim Mağarası (Alanya) Araştırma Raporu, Mimari Ve Elektrikasyon Uygulama Projeleri. General Directorate of Mineral Research and Exploration, Ankara, Turkey.
Hartland, A., Fairchild, I.J., Lead, J.R., Borsato, A., Baker, A., Frisia, S., Baalousha, M., 2012. From soil to cave: transport of trace metals by natural organic matter in karst dripwaters. Chem. Geol. 304–305, 68–82. https://doi.org/10.1016/j.chemgeo.2012.01.032.
He, M., Cai, Y., Zhang, H., Xue, G., Cheng, X., Lu, Y., Wang, G., Qin, X., Ma, L., Wei, Y., Huang, S., Chang, H., Yan, H., 2021. The impact and implications of aragonite-to-calcite transformation on speleothem trace element composition. Sediment. Geol. 425, 106010 https://doi.org/10.1016/j.sedgeo.2021.106010.
Held, F., Cheng, H., Edwards, R.L., Tüysüz, O., Koç, K., Fleitmann, D., 2024. Dansgaard-Oeschger cycles of the penultimate and last glacial period recorded in stalagmites from Türkiye. Nat. Commun. 15, 1183. https://doi.org/10.1038/s41467-024-45507-5.
Henry, L.G., McManus, J.F., Curry, W.B., Roberts, N.L., Piotrowski, A.M., Keigwin, L.D., 2016. North Atlantic ocean circulation and abrupt climate change during the last glaciation. Science 353, 470–474. https://doi.org/10.1126/science.aaf5529.
Hughes, P.D., Allard, J.L., Woodward, J.C., 2022. The Balkans: glacial landforms prior to the last glacial maximum. European Glacial Landscapes 323–332. https://doi.org/10.1016/b978-0-12-823498-3.00034-0.
James, E.W., Banner, J.L., Hardt, B., 2015. A global model for cave ventilation and seasonal bias in speleothem paleoclimate records. G-cubed 16, 1044–1051. https://doi.org/10.1002/2014GC005658.
Jamieson, R.A., Baldini, J.U.L., Brett, M.J., Taylor, J., Ridley, H.E., Ottley, C.J., Prufer, K.M., Wassenburg, J.A., Scholz, D., Breitenbach, S.F.M., 2016. Intra- and inter-annual uranium concentration variability in a Belizean stalagmite controlled by prior aragonite precipitation: a new tool for reconstructing hydro-climate using aragonitic speleothems. Geochem. Cosmochim. Acta 190, 332–346.
Jamieson, R.A., Baldini, J.U.L., Frappier, A.B., Müller, W., 2015. Volcanic ash fall events identified using principal component analysis of a high-resolution speleothem trace

element dataset. Earth Planet Sci. Lett. 426, 36–45. https://doi.org/10.1016/j.epsl.2015.06.014.
Jouzel, J., Masson-Delmotte, V., Cattani, O., Dreyfus, G., Falourd, S., Hoffmann, G., Minster, B., Nouet, J., Barnola, J.M., Chappellaz, J., Fischer, H., Gallet, J.C., Johnsen, S., Leuenberger, M., Loulergue, L., Luethi, D., Oerter, H., Parrenin, F., Raisbeck, G., Raynaud, D., Schilt, A., Schwander, J., Selmo, E., Souchez, R., Spahni, R., Stauffer, B., Steffensen, J.P., Stenni, B., Stocker, T.F., Tison, J.L., Werner, M., Wolff, E.W., 2007. Orbital and millennial antarctic climate variability over the past 800,000 years. Science 317, 793–796. https://doi.org/10.1126/science.1141038.
Kathayat, G., Cheng, H., Sinha, A., Spötl, C., Edwards, R.L., Zhang, H., Li, X., Yi, L., Ning, Y., Cai, Y., Lui, W.L., Breitenbach, S.F.M., 2016. Indian monsoon variability on millennial-orbital timescales. Sci. Rep. 6, 4–10. https://doi.org/10.1038/srep24374.
Kaushal, N., Breitenbach, S.F.M., Lechleitner, F.A., Sinha, A., Tewari, V.C., Ahmad, S.M., Berkelhammer, M., Band, S., Yadava, M., Ramesh, R., Henderson, G.M., 2018. The Indian summer monsoon from a speleothem δ18O perspective—a review. Quaternary 1, 29. https://doi.org/10.3390/quat1030029.
Kern, O.A., Koutsodendris, A., Allstädt, F.J., Mächtle, B., Peteet, D.M., Kalaitzidis, S., Christanis, K., Pross, J., 2022. A near-continuous record of climate and ecosystem variability in Central Europe during the past 130 kyrs (Marine Isotope Stages 5–1) from Füramoos, southern Germany. Quat. Sci. Rev. 284, 107505 https://doi.org/10.1016/j.quascirev.2022.107505.
Kern, Z., Demény, A., Perşoiu, A., Hatvani, I.G., 2019. Speleothem records from the eastern part of europe and Turkey—discussion on stable oxygen and carbon isotopes. Quaternary 2. https://doi.org/10.3390/quat2030031.
Kim, G.-U., Seo, K.-H., Chen, D., 2019. Climate change over the Mediterranean and current destruction of marine ecosystem. Sci. Rep. 9, 18813 https://doi.org/10.1038/s41598-019-55303-7.
Kindler, P., Guillevic, M., Baumgartner, M., Schwander, J., Landais, A., Leuenberger, M., 2014. Temperature reconstruction from 10 to 120 kyr b2k from the NGRIP ice core. Clim. Past 10, 887–902. https://doi.org/10.5194/cp-10-887-2014.
Klaes, B., Wörner, G., Kremer, K., Simon, K., Kronz, A., Scholz, D., Mueller, C.W., Höschen, C., Struck, J., Arz, H.W., Thiele-Bruhn, S., Schimpf, D., Kilian, R., 2022. High-resolution stalagmite stratigraphy supports the Late Holocene tephrochronology of southernmost Patagonia. Commun Earth Environ 3, 23. https://doi.org/10.1038/s43247-022-00358-0.
Kosiorek, M., Wyszkowski, M., 2019. Effect of neutralising substances on reducing influence of cobalt on the content of selected elements in soil. International Journal of Agronomy 33, 153–159.
Koutsodendris, A., Dakos, V., Fletcher, W.J., Knipping, M., Kotthoff, U., Milner, A.M., Müller, U.C., Kaboth-Bahr, S., Kern, O.A., Kolb, L., Vakhrameeva, P., Wulf, S., Christanis, K., Schmiedl, G., Pross, J., 2023. Atmospheric CO2 forcing on Mediterranean biomes during the past 500 kyrs. Nat. Commun. 14, 1664. https://doi.org/10.1038/s41467-023-37388-x.
Kutterolf, S., Schindlbeck- Belo, J.C., Rohr, I., Rademacher, M., de León, A.C., Eisele, S., Freundt, A., Hernandez, W., Wang, K.L., 2020. The arce tephra: two subsequent paroxysmal plinian eruptions from Coatepeque caldera (El Salvador). J. Volcanol. Geoth. Res. 390, 106673 https://doi.org/10.1016/j.jvolgeores.2019.106673.
Kutzbach, J.E., Chen, G., Cheng, H., Edwards, R.L., Liu, Z., 2014. Potential role of winter rainfall in explaining increased moisture in the Mediterranean and Middle East during periods of maximum orbitally-forced insolation seasonality. Clim. Dynam. 42, 1079–1095. https://doi.org/10.1007/s00382-013-1692-1.
Lechleitner, F.A., Lang, S.Q., Haghipour, N., McIntyre, C., Baldini, J.U.L., Prufer, K.M., Eglinton, T.I., 2019. Towards organic carbon isotope records from stalagmites: coupled δ13C and 14C analysis using wet chemical oxidation. Radiocarbon 61, 749–764. https://doi.org/10.1017/RDC.2019.35.
Lézine, A.-M., Izumi, K., Kageyama, M., Achoundong, G., 2019. A 90,000-year record of Afromontane forest responses to climate change. Science 363, 177–181. https://doi.org/10.1126/science.aav6821.
Li, C., Born, A., 2019. Coupled atmosphere-ice-ocean dynamics in Dansgaard-Oeschger events. Quat. Sci. Rev. 203, 1–20. https://doi.org/10.1016/j.quascirev.2018.10.031.
Lisiecki, L.E., Raymo, M.E., 2005. A Pliocene-Pleistocene stack of 57 globally distributed benthic δ 18O records. Paleoceanography 20, 1–17. https://doi.org/10.1029/2004PA001071.
Litt, T., Pickarski, N., Heumann, G., Stockhecke, M., Tzedakis, P.C., 2014. A 600,000 year long continental pollen record from Lake Van, eastern Anatolia (Turkey). Quat. Sci. Rev. 104, 30–41. https://doi.org/10.1016/j.quascirev.2014.03.017.
Lynch-Stieglitz, J., 2017. The atlantic meridional overturning circulation and abrupt climate change. Ann. Rev. Mar. Sci 9, 83–104. https://doi.org/10.1146/annurev-marine-010816-060415.
Martinez-Villalobos, C., Neelin, J.D., 2023. Regionally high risk increase for precipitation extreme events under global warming. Sci. Rep. 13, 5579. https://doi.org/10.1038/s41598-023-32372-3.
Marvel, K., Cook, B.I., Bonfils, C.J.W., Durack, P.J., Smerdon, J.E., Williams, A.P., 2019. Twentieth-century hydroclimate changes consistent with human influence. Nature 569, 59–65. https://doi.org/10.1038/s41586-019-1149-8.
McMillan, E.A., Fairchild, I.J., Frisia, S., Borsato, A., McDermott, F., 2005. Annual trace element cycles in calcite-aragonite speleothems: evidence of drought in the western Mediterranean 1200-1100 yr BP. J. Quat. Sci. 20, 423–433. https://doi.org/10.1002/jqs.943.
Medyńska-Juraszek, A., Ćwieląg-Piasecka, I., Jerzykiewicz, M., Trynda, J., 2020. Wheat straw biochar as a specific sorbent of cobalt in soil. Materials 13, 2462.
Mehterian, S., Pourmand, A., Sharifi, A., Lahijani, H.A.K., Naderi, M., Swart, P.K., 2017. Speleothem records of glacial/interglacial climate from Iran forewarn of future Water Availability in the interior of the Middle East. Quat. Sci. Rev. 164, 187–198. https://doi.org/10.1016/j.quascirev.2017.03.028.
Menviel, L.C., Skinner, L.C., Tarasov, L., Tzedakis, P.C., 2020. An ice–climate oscillatory framework for Dansgaard–Oeschger cycles. Nat. Rev. Earth Environ. 1, 677–693. https://doi.org/10.1038/s43017-020-00106-y.
Miebach, A., Stolzenberger, S., Wacker, L., Hense, A., Litt, T., 2019. A new Dead Sea pollen record reveals the last glacial paleoenvironment of the southern Levant. Quat. Sci. Rev. 214, 98–116. https://doi.org/10.1016/j.quascirev.2019.04.033.
Miller, C.S., Gosling, W.D., Kemp, D.B., Coe, A.L., Gilmour, I., 2016. Drivers of ecosystem and climate change in tropical West Africa over the past ~540 000 years. J. Quat. Sci. 31, 671–677. https://doi.org/10.1002/jqs.2893.
Miller, G.H., Geirsdóttir, Á., Zhong, Y., Larsen, D.J., Otto-Bliesner, B.L., Holland, M.M., Bailey, D.A., Refsnider, K.A., Lehman, S.J., Southon, J.R., Anderson, C., Björnsson, H., Thordarson, T., 2012. Abrupt onset of the Little Ice Age triggered by volcanism and sustained by sea-ice/ocean feedbacks. Geophys. Res. Lett. 39, 1–5. https://doi.org/10.1029/2011GL050168.
Mondal, S., Mishra, K.A., Leung, R., Cook, B., 2023. Global droughts connected by linkages between drought hubs. Nat. Commun. 14, 144. https://doi.org/10.1038/s41467-022-35531-8.
Moseley, G.E., Spötl, C., Svensson, A., Cheng, H., Brandstätter, S., Edwards, R.L., 2014. Multi-speleothem record reveals tightly coupled climate between central Europe and Greenland during Marine Isotope Stage 3. Geology 42, 1043–1046. https://doi.org/10.1130/G36063.1.
Mueller, A.D., Anselmetti, F.S., Ariztegui, D., Brenner, M., Hodell, D.A., Curtis, J.H., Escobar, J., Gilli, A., Grzesik, D.A., Guilderson, T.P., Kutterolf, S., Plötze, M., 2010. Late Quaternary palaeoenvironment of northern Guatemala: evidence from deep drill cores and seismic stratigraphy of Lake Petén Itzá. Sedimentology 57, 1220–1245. https://doi.org/10.1111/j.1365-3091.2009.01144.x.
Müller, W., Shelley, M., Miller, P., Broude, S., 2009. Initial performance metrics of a new custom-designed ArF excimer LA-ICPMS system coupled to a two-volume laser-ablation cell. J. Anal. Atomic Spectrom. 24, 209.
Okay, A.I., Özgül, N., 1984. HP/LT metamorphism and the structure of the Alanya Massif. In: Geological Evolution of the Eastern Mediterranean. Blackwell, London.
Paine, A.R., Baldini, J.U.L., Wadsworth, F.B., Lechleitner, F.A., Jamieson, R.A., Baldini, L.M., Brown, R.J., Müller, W., Hercman, H., Gąsiorowski, M., Stefaniak, K., Socha, P., Sobczyk, A., Kasprzak, M., 2021a. The trace-element composition of a Polish stalagmite: implications for the use of speleothems as a record of explosive volcanism. Chem. Geol. 570 https://doi.org/10.1016/j.chemgeo.2021.120157.
Paine, A.R., Wadsworth, F.B., Baldini, J.U.L., 2021b. Supereruption doublet at a climate transition. Communications Earth & Environment 2, 219–221. https://doi.org/10.1038/s43247-021-00293-6.
Panagiotopoulos, K., Böhm, A., Leng, M.J., Wagner, B., Schäbitz, F., 2014. Climate variability over the last 92 ka in SW Balkans from analysis of sediments from Lake Prespa. Clim. Past 10, 643–660. https://doi.org/10.5194/cp-10-643-2014.
Past Interglacials Working Group of PAGES, 2016. Interglacials of the last 800,000 years. Rev. Geophys. 54, 162–219. https://doi.org/10.1002/2015RG000482.
Pearson, A.R., Hartland, A., Frisia, S., Fox, B.R.S., 2020. Formation of calcite in the presence of dissolved organic matter: partitioning, fabrics and fluorescence. Chem. Geol. 539, 119492 https://doi.org/10.1016/j.chemgeo.2020.119492.
Perez-Espinosa, A., Moral, R., Moreno-Caselles, J., Cortes, A., Perez-Murcia, M.D., Gomez, I., 2005. Co phytoavailability for tomato in amended calcareous soils. Bioresour. Technol. 96, 649–655.
Pickarski, N., Kwiecien, O., Langgut, D., Litt, T., 2015. Abrupt climate and vegetation variability of eastern Anatolia during the last glacial. Clim. Past 11, 1491–1505. https://doi.org/10.5194/cp-11-1491-2015.
Polyak, V.J., Asmerom, Y., Lachniet, M.S., 2017. Rapid speleothem δ 13 C change in southwestern North America coincident with Greenland stadial 20 and the Toba (Indonesia) supereruption. Geology 45 (1), 843–846. https://doi.org/10.1130/G39149.
Railsback, L.B., Gibbard, P.L., Head, M.J., Voarintsoa, N.R.G., Toucanne, S., 2015. An optimized scheme of lettered marine isotope substages for the last 1.0 million years, and the climatostratigraphic nature of isotope stages and substages. Quat. Sci. Rev. 111, 94–106. https://doi.org/10.1016/j.quascirev.2015.01.012.
Rasmussen, S.O., Bigler, M., Blockley, S.P., Blunier, T., Buchardt, S.L., Clausen, H.B., Cvijanovic, I., Dahl-Jensen, D., Johnsen, S.J., Fischer, H., Gkinis, V., Guillevic, M., Hoek, W.Z., Lowe, J.J., Pedro, J.B., Popp, T., Seierstad, I.K., Steffensen, J.P., Svensson, A.M., Vallelonga, P., Vinther, B.M., Walker, M.J.C., Wheatley, J.J., Winstrup, M., 2014. A stratigraphic framework for abrupt climatic changes during the Last Glacial period based on three synchronized Greenland ice-core records: refining and extending the INTIMATE event stratigraphy. Quat. Sci. Rev. 106, 14–28. https://doi.org/10.1016/j.quascirev.2014.09.007.
Ravichandran, M., 2004. Interactions between mercury and dissolved organic matter - a review. Chemosphere 55, 319–331. https://doi.org/10.1016/j.chemosphere.2003.11.011.
Regattieri, E., Zanchetta, G., Drysdale, R.N., Isola, I., Woodhead, J.D., Hellstrom, J.C., Giaccio, B., Greig, A., Baneschi, I., Dotsika, E., 2016. Environmental variability between the penultimate deglaciation and the mid Eemian: insights from Tana che Urla (central Italy) speleothem trace element record. Quat. Sci. Rev. 152, 80–92. https://doi.org/10.1016/j.quascirev.2016.09.027.
Ridley, H.E., Asmerom, Y., Baldini, J.U.L., Breitenbach, S.F.M., Aquino, V.V., Prufer, K.M., Culleton, B.J., Polyak, V., Lechleitner, F.A., Kennett, D.J., Zhang, M., Marwan, N., Macpherson, C.G., Baldini, L.M., Xiao, T., Peterkin, J.L., Awe, J., Haug, G.H., 2015. Aerosol forcing of the position of the intertropical convergence zone since ad 1550. Nat. Geosci. 8, 195–200. https://doi.org/10.1038/ngeo2353.
Rohling, E.J., Marino, G., Grant, K.M., 2015. Mediterranean climate and oceanography, and the periodic development of anoxic events (sapropels). Earth Sci. Rev. 143, 62–97. https://doi.org/10.1016/j.earscirev.2015.01.008.

Rowe, P.J., Mason, J.E., Andrews, J.E., Marca, A.D., Thomas, L., Van Calsteren, P., Jex, C.N., Vonhof, H.B., Al-Omari, S., 2012. Speleothem isotopic evidence of winter rainfall variability in northeast Turkey between 77 and 6 ka. Quat. Sci. Rev. 45, 60–72. https://doi.org/10.1016/j.quascirev.2012.04.013.

Rowe, P.J., Wickens, L.B., Sahy, D., Marca, A.D., Peckover, E., Noble, S., Özkul, M., Baykara, M.O., Millar, I.L., Andrews, J.E., 2020. Multi-proxy speleothem record of climate instability during the early last interglacial in southern Turkey. Palaeogeogr. Palaeoclimatol. Palaeoecol. 538, 109422 https://doi.org/10.1016/j.palaeo.2019.109422.

Sadori, L., Koutsodendris, A., Panagiotopoulos, K., Masi, A., Bertini, A., Combourieu-Nebout, N., Francke, A., Kouli, K., Joannin, S., Mercuri, A.M., Peyron, O., Torri, P., Wagner, B., Zanchetta, G., Sinopoli, G., Donders, T.H., 2016. Pollen-based paleoenvironmental and paleoclimatic change at Lake Ohrid (south-eastern Europe) during the past 500 ka. Biogeosciences 13, 1423–1437. https://doi.org/10.5194/bg-13-1423-2016.

Schaebitz, F., Asrat, A., Lamb, H.F., Cohen, A.S., Foerster, V., Duesing, W., Kaboth-Bahr, S., Opitz, S., Viehberg, F.A., Vogelsang, R., Dean, J., Leng, M.J., Junginger, A., Ramsey, C.B., Chapot, M.S., Deino, A., Lane, C.S., Roberts, H.M., Vidal, C., Tiedemann, R., Trauth, M.H., 2021. Hydroclimate changes in eastern Africa over the past 200,000 years may have influenced early human dispersal. Communications Earth & Environment 2. https://doi.org/10.1038/s43247-021-00195-7.

Scholz, C.A., Johnson, T.C., Cohen, A.S., King, J.W., Peck, J.A., Overpeck, J.T., Talbot, M. R., Brown, E.T., Kalindekafe, L., Amoako, P.Y.O., Lyons, R.P., Shanahan, T.M., Castañeda, I.S., Heil, C.W., Forman, S.L., McHargue, L.R., Beuning, K.R., Gomez, J., Pierson, J., 2007. East African megadroughts between 135 and 75 thousand years ago and bearing on early-modern human origins. Proc. Natl. Acad. Sci. U.S.A. 104, 16416–16421. https://doi.org/10.1073/pnas.0703874104.

Sherwin, C.M., Baldini, J.U.L., 2011. Cave air and hydrological controls on prior calcite precipitation and stalagmite growth rates: implications for palaeoclimate reconstructions using speleothems. Geochem. Cosmochim. Acta 75, 3915–3929. https://doi.org/10.1016/j.gca.2011.04.020.

Slawinska, J., Robock, A., 2018. Impact of volcanic eruptions on decadal to centennial fluctuations of Arctic sea ice extent during the Last Millennium and on initiation of the Little Ice Age. J. Clim. 31, 2145–2167. https://doi.org/10.1175/JCLI-D-16-0498.1.

Sliwinski, J.T., Kost, O., Endres, L., Iglesias, M., Haghipour, N., González-Lemos, S., Stoll, H.M., 2023. Exploring soluble and colloidally transported trace elements in stalagmites: the strontium-yttrium connection. Geochem. Cosmochim. Acta 343, 64–83. https://doi.org/10.1016/j.gca.2022.12.023.

Srivastava, P., Bolan, N., Casagrande, V., Benjamin, J., Adejumo, S.A., Sabir, M., Farooqi, Z.-R., Saifullah, 2022. Cobalt in soils: sources, fate, bioavailability, plant uptake, remediation, and management. In: Appraisal of Metal (Loids) in the Ecosystem. Elsevier, pp. 81–104. https://doi.org/10.1016/B978-0-323-85621-8.00007-8.

Stockhecke, M., Timmermann, A., Kipfer, R., Haug, G.H., Kwiecien, O., Friedrich, T., Menviel, L., Litt, T., Pickarski, N., Anselmetti, F.S., 2016. Millennial to orbital-scale variations of drought intensity in the Eastern Mediterranean. Quat. Sci. Rev. 133, 77–95. https://doi.org/10.1016/j.quascirev.2015.12.016.

Stoll, H.M., Cacho, I., Gasson, E., Sliwinski, J., Kost, O., Iglesias, M., Torner, J., Perez-mejias, C., Haghipour, N., Cheng, H., Edwards, R.L., Moreno, A., 2022. Rapid northern hemisphere ice sheet melting during the penultimate deglaciation. Nat. Commun. 13, 3819. https://doi.org/10.1038/s41467-022-31619-3.

Stoll, H.M., Müller, W., Prieto, M., 2012. I-STAL, a model for interpretation of Mg/Ca, Sr/Ca and Ba/Ca variations in speleothems and its forward and inverse application on seasonal to millennial scales. G-cubed 13, 1–27. https://doi.org/10.1029/2012GC004183.

Storey, M., Roberts, R.G., Saidin, M., 2012. Astronomically calibrated 40 Ar/39 Ar age for the Toba supereruption and global synchronization of late Quaternary records. Proc. Natl. Acad. Sci. USA 109, 18684–18688. https://doi.org/10.1073/pnas.1208178109.

Sun, Y., McManus, J.F., Clemens, S.C., Zhang, X., Vogel, H., Hodell, D.A., Guo, F., Wang, T., Liu, X., An, Z., 2021. Persistent orbital influence on millennial climate variability through the Pleistocene. Nat. Geosci. 14, 812–818. https://doi.org/10.1038/s41561-021-00794-1.

Tan, L., Shen, C.C., Cai, Y., Lo, L., Cheng, H., An, Z., 2014. Trace-element variations in an annually layered stalagmite as recorders of climatic changes and anthropogenic pollution in central China. Quaternary Research (United States) 81, 181–188. https://doi.org/10.1016/j.yqres.2013.12.001.

Timmermann, A., Yun, K.-S., Raia, P., Ruan, J., Mondanaro, A., Zeller, E., Zollikofer, C., Ponce De León, M., Lemmon, D., Willeit, M., Ganopolski, A., 2022. Climate effects on archaic human habitats and species successions. Nature 604, 495–501. https://doi.org/10.1038/s41586-022-04600-9.

Treble, P.C., Shelley, J.M.G., Chappell, J., 2003. Comparison of high-resolution sub-annual records of trace elements in a modern (1911–1992) speleothem with instrumental climate data from southwest Australia. Earth Planet Sci. Lett. 216, 141–153.

Újvári, G., Kovács, J., Varga, G., Raucsik, B., Marković, S.B., 2010. Dust flux estimates for the Last Glacial Period in East Central Europe based on terrestrial records of loess deposits: a review. Quat. Sci. Rev. 29, 3157–3166. https://doi.org/10.1016/j.quascirev.2010.07.005.

Ünal-Imer, E., Shulmeister, J., Zhao, J.X., Tonguç Uysal, I., Feng, Y.X., Duc Nguyen, A., Yüce, G., 2015. An 80 kyr-long continuous speleothem record from Dim Cave, SW Turkey with paleoclimatic implications for the Eastern Mediterranean. Sci. Rep. 5, 1–11. https://doi.org/10.1038/srep13560.

Ünal-Imer, E., Shulmeister, J., Zhao, J.X., Uysal, I.T., Feng, Y.X., 2016. High-resolution trace element and stable/radiogenic isotope profiles of late Pleistocene to Holocene speleothems from Dim Cave, SW Turkey. Palaeogeogr. Palaeoclimatol. Palaeoecol. 452, 68–79. https://doi.org/10.1016/j.palaeo.2016.04.015.

Vaks, A., Bar-Matthews, M., Ayalon, A., Matthews, A., Frumkin, A., Dayan, U., Halicz, L., Almogi-Labin, A., Schilman, B., 2006. Paleoclimate and location of the border between Mediterranean climate region and the Saharo–Arabian Desert as revealed by speleothems from the northern Negev Desert, Israel. Earth Planet Sci. Lett. 249, 384–399. https://doi.org/10.1016/j.epsl.2006.07.009.

Vaks, A., Bar-Matthews, M., Matthews, A., Ayalon, A., Frumkin, A., 2010. Middle-Late quaternary paleoclimate of northern margins of the saharan-arabian desert: reconstruction from speleothems of negev desert, Israel. Quat. Sci. Rev. 29, 2647–2662. https://doi.org/10.1016/j.quascirev.2010.06.014.

Verniers, T., Couper, H., Lechleitner, F.A., Baldini, J.U.L., 2022. Southeast Asian dust flux reconstructed using accurately dated stalagmite thorium concentrations. Results in Geochemistry 7–8, 100017. https://doi.org/10.1016/j.ringeo.2022.100017.

Wagner, B., Leng, M.J., Wilke, T., Böhm, A., Panagiotopoulos, K., Vogel, H., Lacey, J.H., Zanchetta, G., Sulpizio, R., 2014. Distinct lake level lowstand in Lake Prespa (SE Europe) at the time of the 74 (75) ka Toba eruption. Clim. Past 10, 261–267. https://doi.org/10.5194/cp-10-261-2014.

Wagner, B., Vogel, H., Francke, A., Friedrich, T., Donders, T., Lacey, J.H., Leng, M.J., Regattieri, E., Sadori, L., Wilke, T., Zanchetta, G., Albrecht, C., Bertini, A., Combourieu-Nebout, N., Cvetkoska, A., Giaccio, B., Grazhdani, A., Hauffe, T., Holtvoeth, J., Joannin, S., Jovanovska, E., Just, J., Kouli, K., Kousis, I., Koutsodendris, A., Krastel, S., Lagos, M., Leicher, N., Levkov, Z., Lindhorst, K., Masi, A., Melles, M., Mercuri, A.M., Nomade, S., Nowaczyk, N., Panagiotopoulos, K., Peyron, O., Reed, J.M., Sagnotti, L., Sinopoli, G., Stelbrink, B., Sulpizio, R., Timmermann, A., Tofilovska, S., Torri, P., Wagner-Cremer, F., Wonik, T., Zhang, X., 2019. Mediterranean winter rainfall in phase with African monsoons during the past 1.36 million years. Nature 573, 256–260. https://doi.org/10.1038/s41586-019-1529-0.

Waldmann, N., Stein, M., Ariztegui, D., Starinsky, A., 2009. Stratigraphy, depositional environments and level reconstruction of the last interglacial Lake Samra in the Dead Sea basin. Quat. res. 72, 1–15. https://doi.org/10.1016/j.yqres.2009.03.005.

Wang, X., Auler, A.S., Edwards, R.L., Cheng, H., Ito, E., Solheid, M., 2006. Interhemispheric anti-phasing of rainfall during the last glacial period. Quat. Sci. Rev. 25, 3391–3403. https://doi.org/10.1016/j.quascirev.2006.02.009.

Wang, Y.J., Cheng, H., Edwards, R.L., An, Z.S., Wu, J.Y., Shen, C.-C., Dorale, J.A., 2001. A high-resolution absolute-dated Late Pleistocene monsoon record from Hulu Cave, China. Science 294, 2345–2348.

Wassenburg, J.A., Immenhauser, A., Richter, D.K., Jochum, K.P., Fietzke, J., Deininger, M., Goos, M., Scholz, D., Sabaoui, A., 2012. Climate and cave control on Pleistocene/Holocene calcite-to-aragonite transitions in speleothems from Morocco: elemental and isotopic evidence. Geochem. Cosmochim. Acta 92, 23–47. https://doi.org/10.1016/j.gca.2012.06.002.

Wassenburg, J.A., Riechelmann, S., Schröder-Ritzrau, A., Riechelmann, D.F.C., Richter, D.K., Immenhauser, A., Terente, M., Constantin, S., Hachenberg, A., Hansen, M., Scholz, D., 2020. Calcite Mg and Sr partition coefficients in cave environments: implications for interpreting prior calcite precipitation in speleothems. Geochem. Cosmochim. Acta 269, 581–596. https://doi.org/10.1016/j.gca.2019.11.011.

Wassenburg, J.A., Scholz, D., Jochum, K.P., Cheng, H., Oster, J., Immenhauser, A., Richter, D.K., Häger, T., Jamieson, R.A., Baldini, J.U.L., Hoffmann, D., Breitenbach, S.F.M., 2016. Determination of aragonite trace element distribution coefficients from speleothem calcite–aragonite transitions. Geochem. Cosmochim. Acta 190, 347–367. https://doi.org/10.1016/j.gca.2016.06.036.

Wong, C.I., Breecker, D.O., 2015. Advancements in the use of speleothems as climate archives. Quat. Sci. Rev. 127, 1–18. https://doi.org/10.1016/j.quascirev.2015.07.019.

Zhang, X., Barker, S., Knorr, G., Lohmann, G., Drysdale, R., Sun, Y., Hodell, D., Chen, F., 2021. Direct astronomical influence on abrupt climate variability. Nat. Geosci. 14, 819–826. https://doi.org/10.1038/s41561-021-00846-6.

Zhong, Y., Miller, G.H., Otto-Bliesner, B.L., Holland, M.M., Bailey, D.A., Schneider, D.P., Geirsdóttir, Á., 2011. Centennial scale climate change from decadally-paced explosive volcanism: a coupled sea ice-ocean mechanism. Clim. Dynam. 37, 2373–2387.

Zhornyak, L.V., Zanchetta, G., Drysdale, R.N., Hellstrom, J.C., Isola, I., Regattieri, E., Piccini, L., Baneschi, I., Couchoud, I., 2011. Stratigraphic evidence for a "pluvial phase" between ca 8200–7100 ka from Renella cave (Central Italy). Quat. Sci. Rev. 30, 409–417. https://doi.org/10.1016/j.quascirev.2010.12.003.

Zhou, H., Chi, B., Lawrence, M., Zhao, J., Yan, J., Greig, A., Feng, Y., 2008a. High resolution and precisely dated record of weathering and hydrological dynamics recorded by manganese and rare earth elements in a stalagmite from central China. Quat. Res. 68, 438–446.

Zhou, H., Greig, A., Tang, J., You, C.F., Yuan, D., Tong, X., Huang, Y., 2012. Rare earth element patterns in a Chinese stalagmite controlled by sources and scavenging from karst groundwater. Geochem. Cosmochim. Acta 83, 1–18. https://doi.org/10.1016/j.gca.2011.12.027.

Zhou, H., Wang, Q., Zhao, J., Zheng, L., Guan, H., Feng, Y., Greig, A., 2008b. Rare earth elements and yttrium in a stalagmite from Central China and potential paleoclimatic implications. Palaeogeogr. Palaeoclimatol. Palaeoecol. 207, 128–138.

Zimmerer, M.J., Lafferty, J., Coble, M.A., 2016. The eruptive and magmatic history of the youngest pulse of volcanism at the Valles caldera: implications for successfully dating late Quaternary eruptions. J. Volcanol. Geoth. Res. 310, 50–57. https://doi.org/10.1016/j.jvolgeores.2015.11.021.

Zittis, G., Almazroui, M., Alpert, P., Ciais, P., Cramer, W., Dahdal, Y., Fnais, M., Francis, D., Hadjinicolaou, P., Howari, F., Jrrar, A., Kaskaoutis, D.G., Kulmala, M., Lazoglou, G., Mihalopoulos, N., Lin, X., Rudich, Y., Sciare, J., Stenchikov, G.,

Xoplaki, E., Lelieveld, J., 2022. Climate change and weather extremes in the eastern mediterranean and Middle East. Rev. Geophys. 60 https://doi.org/10.1029/2021RG000762.